SMC-TR-98-04

AEROSPACE REPORT NO.
TR-98(1410)-1

# Titan 34D-9 Abort Cloud Measurements—Quantitative Imagery from Two Camera Sites

20 February 1998

Prepared by

R. N. ABERNATHY
Space and Environment Technology Center
Technology Operations



Prepared for

SPACE AND MISSILE SYSTEMS CENTER
AIR FORCE MATERIEL COMMAND
2430 E. El Segundo Boulevard
Los Angeles Air Force Base, CA 90245

Space Systems Group



THE AEROSPACE CORPORATION
El Segundo, California

This report was submitted by The Aerospace Corporation, El Segundo, CA 90245-4691, under Contract No. F04701-93-C-0094 with the Space and Missile Systems Center, 2430 E. El Segundo Blvd., Los Angeles Air Force Base, CA 90245. It was reviewed and approved for The Aerospace Corporation by A. B. Christensen, Principal Director, Space and Environment Technology Center. Capt. Brian Laine was the project officer for the program.

This report has been reviewed by the Public Affairs Office (PAS) and is releasable to the National Technical Information Service (NTIS). At NTIS, it will be available to the general public, including foreign nationals.

This technical report has been reviewed and is approved for publication. Publication of this report does not constitute Air Force approval of the report's findings or conclusions. It is published only for the exchange and stimulation of ideas.

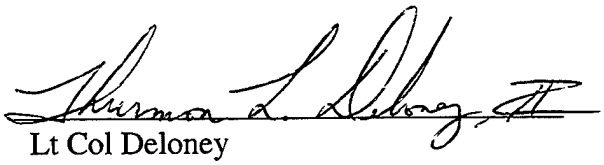

Lt Col Deloney
SMC/CLNE

# REPORT DOCUMENTATION PAGE

*Form Approved*
*OMB No. 0704-0188*



| 1. AGENCY USE ONLY (*Leave blank*) | 2. REPORT DATE | 3. REPORT TYPE AND DATES COVERED |
|---|---|---|
| | 20 February 1998 | |

4. TITLE AND SUBTITLE
Titan 34D-9 Abort Cloud Measurements—Quantitative Imagery from Two Camera Sites

5. FUNDING NUMBERS
F04701-93-C-0094

6. AUTHOR(S)
R. N. Abernathy

7. PERFORMING ORGANIZATION NAME(S) AND ADDRESS(ES)
The Aerospace Corporation
Technology Operations
El Segundo, CA 90245-4691

8. PERFORMING ORGANIZATION REPORT NUMBER
TR-98(1410)-1

9. SPONSORING/MONITORING AGENCY NAME(S) AND ADDRESS(ES)
Space and Missile Systems Center
Air Force Materiel Command
2430 E. El Segundo Boulevard
Los Angeles Air Force Base, CA 90245

10. SPONSORING/MONITORING AGENCY REPORT NUMBER
SMC-TR-98-04

11. SUPPLEMENTARY NOTES

12a. DISTRIBUTION/AVAILABILITY STATEMENT
Approved for public release; distribution unlimited

12b. DISTRIBUTION CODE

13. ABSTRACT (*Maximum 200 words*)

The low-altitude explosion of the Titan 34D-9 on 18 April 1986 at Vandenberg Air Force Base provides a unique opportunity to test and validate toxic cloud transport models for the near-ground catastrophic abort scenario. Video tape imagery of the 34D-9 abort cloud from two sites at VAFB has been analyzed using techniques developed to track and measure the ground clouds from normal launches. Since abort cloud transport model predictions have been responsible for launch holds and delays at both the Eastern and Western ranges, these data are an important complement to the more extensive normal launch data. We calculated the 34D-9 abort cloud's air entrainment coefficient using cloud volumes and altitudes derived from imagery. The assumptions used in processing the imagery are consistent with T-0.5 hour rawinsonde data. The entrainment coefficient is the slope of a plot of the cloud's sphere-equivalent radius vs altitude. It is a critical input parameter in the Rocket Exhaust Effluent Dispersion Model (REEDM) used by both ranges to predict toxic cloud transport. The entrainment coefficient (0.35±0.01) for the Titan 34D-9 abort cloud is in good agreement with the imagery-derived values for normal Titan IV launch clouds.

14. SUBJECT TERMS
Toxic launch cloud, Toxic hazard corridors, Atmospheric dispersion models, Launch abort cloud, Development and dispersion, Launch abort cloud imagery, $N_2O_4$ monitoring, Titan 34D-9

15. NUMBER OF PAGES
47

16. PRICE CODE

| 17. SECURITY CLASSIFICATION OF REPORT | 18. SECURITY CLASSIFICATION OF THIS PAGE | 19. SECURITY CLASSIFICATION OF ABSTRACT | 20. LIMITATION OF ABSTRACT |
|---|---|---|---|
| UNCLASSIFIED | UNCLASSIFIED | UNCLASSIFIED | |

## Acknowledgments

The Air Force Space and Missile Systems Center's Launch Programs Office (SMC/CL) is sponsoring the Atmospheric Dispersion Model Validation Program (MVP). This program is collecting launch cloud dispersion data that will be used to determine the accuracy of atmospheric dispersion models, such as REEDM, in predicting toxic hazard corridors at the launch ranges. This report reviews launch cloud imagery and meteorological measurements performed during the Titan 34D-9 failure at Vandenberg Air Force Base on 18 April 1986.

An MVP Integrated Product Team (IPT) led by Capt. Brian Laine (SMC/CLNM) is directing the MVP effort. Dr. Bart Lundblad of The Aerospace Corporation's Environmental Systems Directorate (ESD) is the MVP technical manager.

Dr. Robert N. Abernathy, Dr. J. T. Knudtson, Mr. Brian P. Kasper, and Ms. Karen L. Foster of The Aerospace Corporation's Environmental Monitoring and Technology Department (EMTD) reviewed visible imagery acquired from Mr. M. Buechler of The Aerospace Corporation's Propulsive Systems Directorate. Mr. J. F. Kephart of The Aerospace Corporation's Western Range Office provided valuable range-specific data required to calibrate and interpret the imagery. Ms. Foster digitized imagery data for analysis by Dr. Abernathy. Mr. Kasper created and maintains the PLMTRACK and PLMVOL programs used by Dr. Abernathy for pairwise analysis of simultaneously acquired imagery from two sites. Dr. Abernathy used Microsoft Excel worksheets to manually process imagery separately for each imagery site and as needed to calibrate the imagery. The description of the cloud imagery results was prepared by Dr. Abernathy.

The meteorological data documented in Appendix E was reconstructed by Geodynamics and was formatted by Dr. Abernathy to conform to REEDM input file requirements. Dr. Abernathy also provided the column headings for the input file to make it useful for other models and modelers.

The 34D-9 analysis represents the first abort cloud measurements collected by the MVP. The MVP has deployed quantitative imagery systems to more than 15 normal launches since 1994. Most of the normal launch measurements were Titan IV vehicles before the solid rocket motor upgrade (SRMU). To date, the measurements also include a Titan IV B (i.e., SRMU), a Peacekeeper, and Atlas launch. The MVP has also used airship releases of non-toxic chemicals to study dispersion as a function of release altitude. All of these data will be used to challenge dispersion models.

## Contents

## Figures

## Figures (Continued)

# Tables

## Executive Summary

The following analysis estimates the rise and growth rates for the Titan 34D-9 abort cloud from visible imagery recorded on 18 April 1986 from two sites on Vandenberg Air Force Base (VAFB). At 10:45 PST, during an apparently normal launch, the Titan 34D-9 exploded about 830 feet above SLC-4E resulting in the deflagration of the hypergolic propellants and the formation of a red abort cloud. The Titan 34D-9 data provide a unique test case for validating dispersion models for the most hazardous abort scenario (i.e., near-ground catastrophic abort). As part of the Model Validation Program (MVP), the analysis of the 34D-9 abort cloud imagery was intended to complement the more extensive exhaust cloud data obtained by quantitative imagery and by aircraft sampling of the "ground" clouds resulting from normal launches.[1-10] By comparing the behavior of the abort cloud to that of the normal launch clouds, one can test model assumptions and approximations to determine if they apply equally to both cases.

This analysis of the Titan 34D-9 incident focused upon the quantitative interpretation of the imagery from the Surf gate site (i.e., north of SLC-4E). The Surf imagery documented the growth and the rise of the abort cloud until 130 seconds after the first visual indication of the solid rocket motor failure. We used imagery from the "Program" site (i.e., east of SLC-4E) to validate assumptions used in the analysis of the Surf imagery and to quantify the aspect ratio (i.e., horizontal to vertical diameter) from the eastern perspective. We estimated the abort cloud's entrainment coefficient using the combined imagery data from both Surf and Program sites as well as the T-0.5 hour rawinsonde data. The entrainment coefficient is the slope of a plot of the cloud's sphere equivalent radius versus altitude. It is a critical parameter in the Rocket Exhaust Effluent Dispersion Model (REEDM).

The entrainment coefficient (0.35 +/- 0.01) for the Titan 34D-9 abort cloud is the equivalent to the entrainment coefficients we have measured for normal launch clouds. Therefore, these data document similar behavior for normal launch clouds and the single abort cloud in regards to this important model parameter. Furthermore, the measured entrainment coefficient is significantly smaller than the default value (0.64) used by REEDM. Our measurements have resulted in a recommendation for changes to REEDM. These changes could increase launch probability without adversely effecting public safety.

# 1. Introduction

Dispersion model predictions have delayed launches from both Cape Canaveral Air Station (CCAS) and Vandenberg Air Force Base (VAFB). Delays occur when the predicted concentrations of toxic gases resulting from a normal or an aborted launch exceed public exposure criteria. The Rocket Exhaust Effluent Dispersion Model (REEDM) predicts the downwind concentrations of toxic gases for various launch vehicles (e.g., Shuttle, Titan, and Delta) for the normal and several abort scenarios. REEDM predictions are deliberately conservative to compensate for uncertainties in the modeling physics. The predictions for the catastrophic low altitude abort scenario are most likely to delay a launch. In this scenario, the launch vehicle explodes near the pad and releases large quantities of hypergolic fuel and oxidizer. The abort scenario is difficult to model and even more difficult to validate. However, as part of the Model Validation Program (MVP), we have acquired video imagery of the Titan 34D-9 explosion that occurred at VAFB in 1986. This explosion was at 830 feet above the launch pad and corresponds well with the worst-case scenario for potential public exposure to toxic gases. We have analyzed the imagery of this explosion in order to measure the actual cloud transport parameters. This analysis provides the basis for tuning a critical REEDM parameter that should result in more accurate launch cloud predictions.

## 1.1 The Titan 34D-9 Incident

The Titan 34D-9 launch appeared to be normal until 8.38 seconds after launch. A fireball appeared on solid rocket motor (SRM) 2 next to the core vehicle and expanded moving SRM 2 up relative to the core and SRM 1 away relative to the core. The thrust vector control system lost pressure and the SRM 1 inadvertent separation destruct system activated. Deflagration burning in SRM 2 was followed by fragmentation and breakup of the core. Command destruct was initiated at T+16.38 seconds. Stage 1 and stage 2 oxidizer clouds were observed within the first second after the first visible mishap thus documenting the rupture of both stages.

The event produced several toxic clouds. The abort cloud contained the $N_2O_4$ oxidizer and was identified by its red color and high altitude. The solid rocket motor exhaust cloud remained below the abort cloud and was white. The burning SRM fragments on the ground produced additional white smoke. Brush fires produced black smoke. The launch pad was SLC-4E which was severely damaged as a result of the explosion that occurred 830 feet above the pad. No deaths resulted from the event, however, 74 people were treated at VAFB hospital for toxic cloud exposure, and three were held overnight for observation. Twenty civilians were exposed to the toxic cloud at Hollister ranch.

The launch was on 18 April 1986 at 18:45:01.110 GMT (10:45 PST). The Titan 34D-9 carried a classified payload and used two 5 ½ segment solid motor boosters as stage 0. The solid motor boosters were manufactured by United Technologies, and each produces 1.4 M LBS thrust at 810 PSIA from Aluminized PBAN. Combined the two 5 ½ segment boosters contained 929,400 LBS of solid propellant. Combined the two TVC systems contained 16,048 LBS of dinitrogen tetroxide ($N_2O_4$). Martin Marietta manufactured the core vehicles that used $N_2O_4$/A-50 hypergolic propellants. Aerozine 50 (A-50) is a 50:50 mixture of anhydrous hydrazine and unsymmetrical dimethyl hydrazine. Aerojet manufactured the engines. Stage 1 contained 103,227 LBS of A-50 and 195,164 LBS of $N_2O_4$. Stage 2 contained 25,038 LBS of A-50 and 44,532 LBS of $N_2O_4$.

## 1.2 34D-9 Imagery

We reviewed several sources of imagery including: television coverage, helicopter videos, pictures from off-coast oil derricks, footage from range cameras, and a civilian video. In order to interpret the imagery quantitatively, we require the following:

1) known location of the imagery site,

2) the time for each image,

3) calibrated field of view (FOV)

4) known pointing angle (i.e., Azimuth and Elevation) to at least one pixel in the image, and

5) complete picture of the abort cloud

Most of the available 34D-9 imagery (i.e., helicopter footage, newscast footage, and amateur photography) was not useful for our purposes since the exact time of each image and the locations of the imagery sites were not recorded. When time and camera site location were known, the imagery often did not include a complete image of the abort cloud or did not include landmarks (i.e., ground features) useful for calibrating the FOV and pointing angle of the image.

Fortunately, an unknown civilian video operator recorded not only excellent footage of the abort cloud but also included landmarks (i.e., the terrain in the imagery). Prior to launch, the civilian at Surf site scanned the terrain and recorded images not only of known landmarks (i.e., SLC-4E and SLC-4W in the same image) but also unknown landmarks (i.e., recognizable features in the terrain). The known landmarks provided absolute calibration of a single video image and all unknown landmarks in that image. These secondary landmarks allowed calibration of subsequent images and tertiary landmarks in those subsequent images. The civilian remained relatively stationary at the Surf site while continuously recording the launch, the abort, and the growth of the abort cloud till 130 seconds after the abort. Our analysis indicates that the abort cloud did not reach its stabilization height during this period.

We found one other site that provided imagery useful for abort cloud measurements. However, the imagery from "Program" site included terrain and the abort cloud in only a couple of short periods (i.e., at about 40 seconds and at about 80 seconds after the abort). The name "Program" has been used over the years for various sites to the east of the launch pads. Through review of the imagery and by interviewing contractor personnel who were on VAFB during the incident, we assigned "Program" to a site near water tank "C" on VAFB. We were able to calibrate the Program site's imagery using the known trajectory of the Titan 34D-9 during the first 8 seconds after launch and unidentified landmarks that appeared in the imagery. Due to the limited amount of imagery from the Program site, we have primarily focused on the interpretation of the Surf site imagery. However the Program site's imagery not only verified the assumptions used to interpret the Surf site's imagery but also provided the aspect ratio from the eastern perspective (i.e., not available from the northern Surf site). When there was simultaneous imagery from both sites, it was possible to calculate the abort cloud volume by triangulating the cloud's position and extent.

Figure 1 is a map of south VAFB that documents the locations of the imagery sites and the launch pads. It is apparent from examination of this map that Surf site was north of the pad and Program Site was east of the pad. Therefore, Surf site provided the vertical and the east/west dimensions of the abort cloud while Program site provided the vertical and the north/south dimensions of the cloud. Likewise, Surf imagery documented any movement in the east/west direction while Program imagery documented movement primarily in the north/south directions. As long as the cloud remained over the pad, either site, alone, documented the rise of the cloud. At later times, when imagery was not available from both sites, the rawinsonde-derived wind direction and speed at cloud altitudes enabled the estimation of the ground track for the abort cloud. When imagery was available from both sites, we triangulated the position and extent of the abort cloud without making any assumptions.

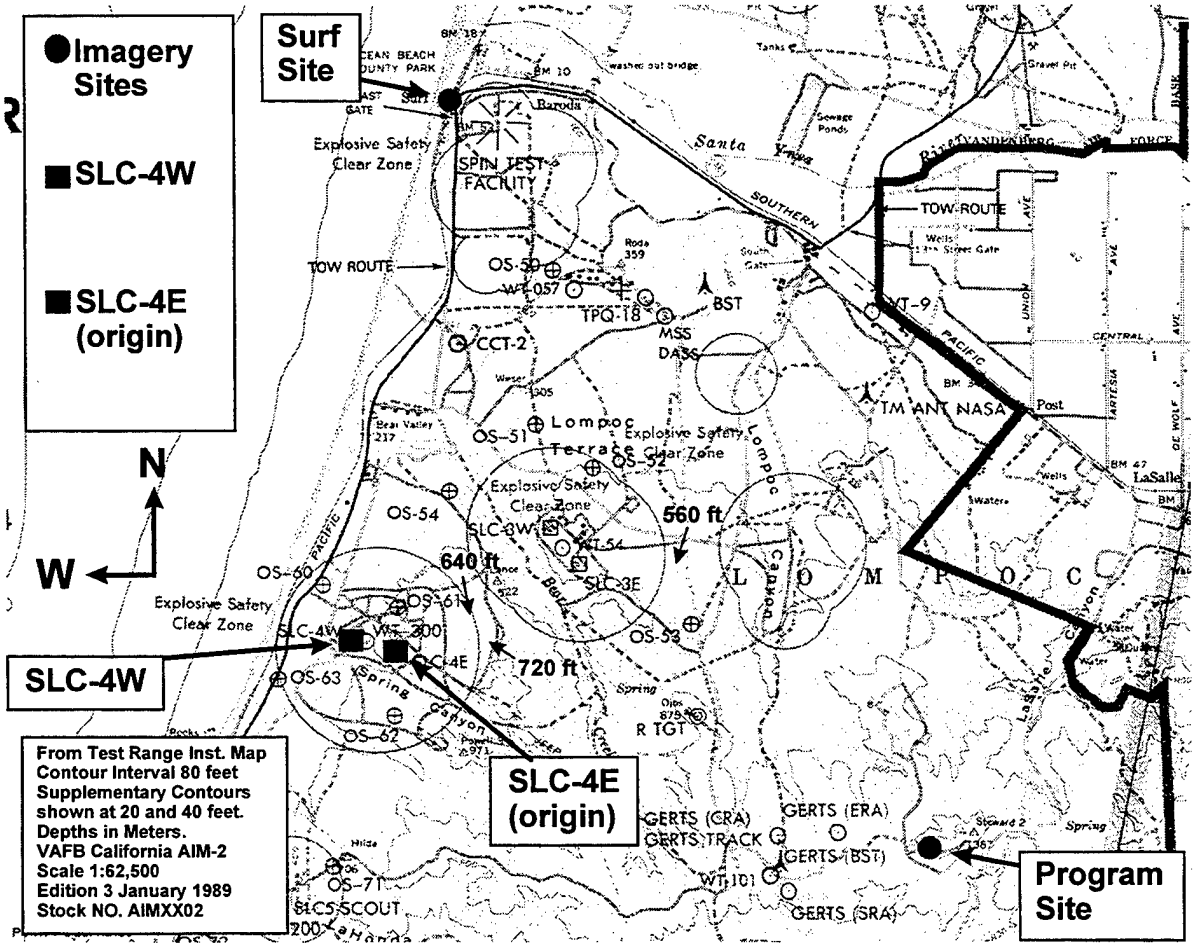


Figure 1. Map documenting south VAFB and 34D-9 imagery sites.

# 2. Analysis

There are several approaches to analyzing imagery. Most involve the interpretation of X and Y pixels in the image as azimuth (AZ) relative to north of the imagery site and elevation (EL) relative to level with the imagery site. The EL can then be used to calculate the height for an object at a known distance from the imagery site. Likewise the angular size of an object (i.e., horizontal diameter in degrees azimuth and vertical diameter in degrees elevation) can be converted to physical dimensions if one knows the distance of the object from the imagery site. Alternatively, when one sees the same object from two sites at the same time, one can calculate the closest approach (i.e., intersection) of the rays defined by the AZ and the EL of the object in the images at each site. The closest approach of such rays triangulates the altitude, latitude, and longitude of the object or feature. We have used all of these approaches to interpret the 34D-9 abort images collected from both Surf and Program sites.

## 2.1 Linear Interpretation of Imagery

The simplest approach is to assume that the X pixels (i.e., horizontal pixels) correspond to azimuth and the Y pixels (i.e., vertical pixels) correspond to elevation. This is an excellent assumption for an image recorded with the camera held horizontal or with a camera only slightly inclined while using a reasonably narrow field of view. The equations used in the linear interpretation of the imagery are:

$$dX \times \text{hdpp} = dAZ \qquad \text{where hdpp = horizontal degrees per X pixel}$$

$$dY \times \text{vdpp} = dEL \qquad \text{where vdpp = vertical degrees per Y pixel}$$

Using known landmarks, one can calculate the azimuth (AZ) and elevation (EL) from the imagery site to each landmark. Therefore, the "X,Y" pixel pair that corresponds to each known landmark is calibrated in terms of AZ and EL from the imagery site. If one has two landmarks in an image, one can calculate the dX and dY (i.e., number of pixels) that correspond to the dAZ and dEL (i.e., number of degrees) between the landmarks. Therefore, one can calculate the hdpp and vdpp (i.e., number of degrees per pixel) for the image for the horizontal and vertical axes. Knowing the total number of horizontal (640) and vertical (480) pixels in the image, one can calculate the horizontal and vertical FOV of the image. Lastly, for any image that is calibrated (i.e., known landmark and known FOV), one can calculate the AZ and EL for any other pixel in the image using the "linear" correlation between dX and dY with dAZ and dEL, respectively.

## 2.2 Trigonometric Interpretation of Imagery

The linear interpretation of the imagery is adequate unless the object is substantially (i.e., 20 or more degrees) above the horizon and significantly (i.e., 10 or more degrees) away from the center of the image. Since the 34D-9 abort cloud remained at low elevations and near the center of the FOV for Surf and Program sites, the linear interpretation should be adequate. However, to eliminate even small errors that might result from the linear interpretation, we present the rigorous trigonometric interpretation of the imagery. It is noteworthy that the simple linear treatment resulted in the same answers.

The failure of the linear interpretation of the imagery is most vividly illustrated by pointing a camera straight up. When pointing straight upward, the center pixel would be at 90 degrees elevation and all

azimuths (they converge at 90 degrees elevation). As one moves away from the center pixel both azimuth and elevation change for all lines except the center "horizontal" axis (i.e., pure X now corresponding to elevation for only this image) and center "elevation" axis (i.e., pure Y corresponding to elevation as with all images).

Figure 2 illustrates a steeply inclined camera (i.e., approximately 45° elevation) and portrays that lines of constant elevation actually curve upward as one moves away from the center of the image. For a level (i.e., 0 degrees tilt) camera, lines of constant elevation appear straight and horizontal. To interpret imagery at elevated angles, one can assume for each row (i.e., constant Y pixel value) in the image that the X pixels correspond linearly to angular rotation within a plane that contains all pixels in that row. Appendix C shows that this allows projection of the angular difference in X pixels to the ground plane using trigonometric identities and the elevation of the plane for that row of pixels. For our purposes, the significance of these corrections is negligible when the difference between the linear and trigonometric methods approaches the pixel size. This was the case for 34D-9 abort cloud imagery from Surf and from Program sites. However, we present the rigorous results in this report.

## 2.3 Single Site Analysis of Imagery

Surf site contained the only useful data for most of its 130 seconds of abort cloud imagery. Surf site's imagery provided the angular elevation and diameters of the abort cloud throughout this period. Using a reasonable assumption that the cloud remained over the pad during this short period, we converted all of Surf site's angular data to lengths (i.e., altitude, horizontal diameter, and vertical diameter) in meters. For this conversion, the known distance between SLC-4E pad and the Surf imagery site was used as the ground distance ($D$) between the abort cloud and Surf site. Analysis of Program imagery and rawinsonde data allowed estimation of better values for $D$ but these corrections had no significant impact on the measured cloud characteristics. Program site's imagery also provided the horizontal to vertical aspect ratio for the abort cloud from an eastern perspective. This

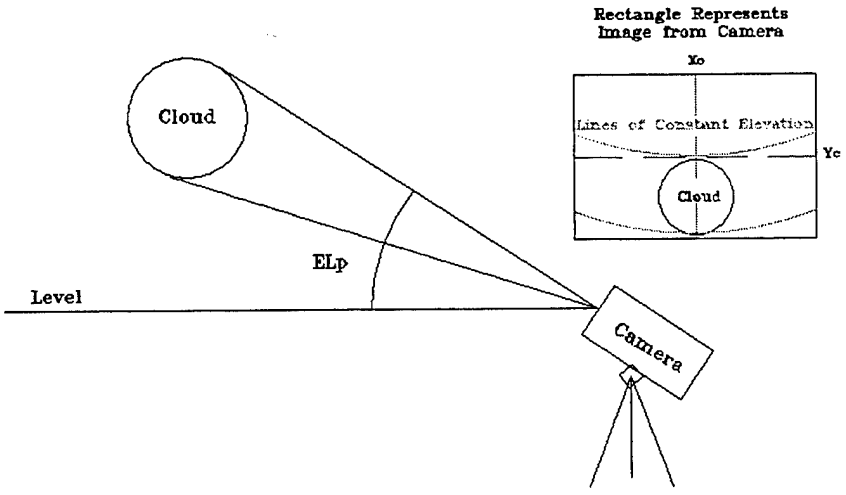


Figure 2. Illustration of curved lines of constant elevation for inclined camera.

complemented Surf site's northern perspective and allowed the estimation of the ellipsoid volume for the abort cloud using measured values for the east/west, north/south, and vertical cloud diameters. All single-site results agree with the triangulated data obtained from stereoscopic analysis. The following sections describe PLMTRACK and PLMVOL which are the stereoscopic analysis algorithms used by The Aerospace Corporation to interpret simultaneous imagery from two or more sites. Appendix D provides additional error analysis for perspective restrictions due to the lookup angle from Surf site. That analysis indicates errors of a 4 to 13% for various cloud parameters.

## 2.4 PLMTRACK Analysis of Imagery from Two Sites

Brian P. Kasper created and maintains the PLMTRACK program at The Aerospace Corporation. PLMTRACK provides a convenient way of triangulating the position of an object using imagery from two sites. In various versions, PLMTRACK has used the linear and rigorous (i.e., trigonometric) methods of interpreting pixels as AZ and EL and vice versa. For the few times when simultaneous imagery was available from both Surf and Program sites, PLMTRACK provided an absolute method of triangulating the position of the abort cloud without making any assumptions regarding the position of the abort cloud. The analyst drew a box about the abort cloud in simultaneously acquired images from both Surf and Program sites. The edges of the box touched the top, left, right, and bottom extremes of the abort cloud as illustrated by Figure 3. PLMTRACK calculated the nearest approach for various rays (i.e., Figure 3) defined by the middle of each of the edges of the boxes and the center of the boxes. These rays define the broadest extent of the cloud in all observable dimensions as illustrated by the Cartesian plot of 34D-9 PLMTRACK results (i.e., for 78.378 s after the abort) in Figure 4. As mentioned previously, this report presents the rigorous trigonometric PLMTRACK results that were similar to the results obtained by the simpler linear algorithm.

The PLMTRACK analysis documented not only the Cartesian extent of the cloud as illustrated in Figure 4 but also the x,y,z coordinates for the top, middle and bottom of the cloud for each pair of images. The PLMTRACK data confirmed that the abort cloud remained over SLC-4E throughout the first 78 seconds after the abort. Therefore, the PLMTRACK analysis validated the assumption used in the single-site processing of the Surf site imagery. Indeed, the results show excellent agreement for the cloud rise data determined by single-site analysis of Surf imagery and PLMTRACK analysis of the combined Surf and Program imagery.

## 2.5 PLMVOL Analysis of Imagery from Two (or More) Sites

Brian P. Kasper also created and maintains the PLMVOL program at The Aerospace Corporation. PLMVOL provides a convenient way of triangulating all of the volume elements that could be occupied by an object using imagery from two (or more) sites. Like PLMTRACK, PLMVOL has used the linear and rigorous (i.e., trigonometric) methods of interpreting pixels as AZ and EL and vice versa. For the few times when simultaneous imagery was available from both Surf and Program sites, the rigorous trigonometric PLMVOL algorithm provided an absolute method of triangulating the position and volume of the abort cloud without making any assumptions. The analyst outlined the edge of the abort cloud in simultaneously acquired images from both Surf and Program sites. PLMVOL determined all of the pixels that were within the outlines in each image and projected the rays for all of those pixels into space. PLMVOL defined volume elements in space and determined which volume elements were intercepted by the projected rays from both imagery sites. These twice intersected volume elements could be occupied by the abort cloud. PLMVOL reports the x,y,z

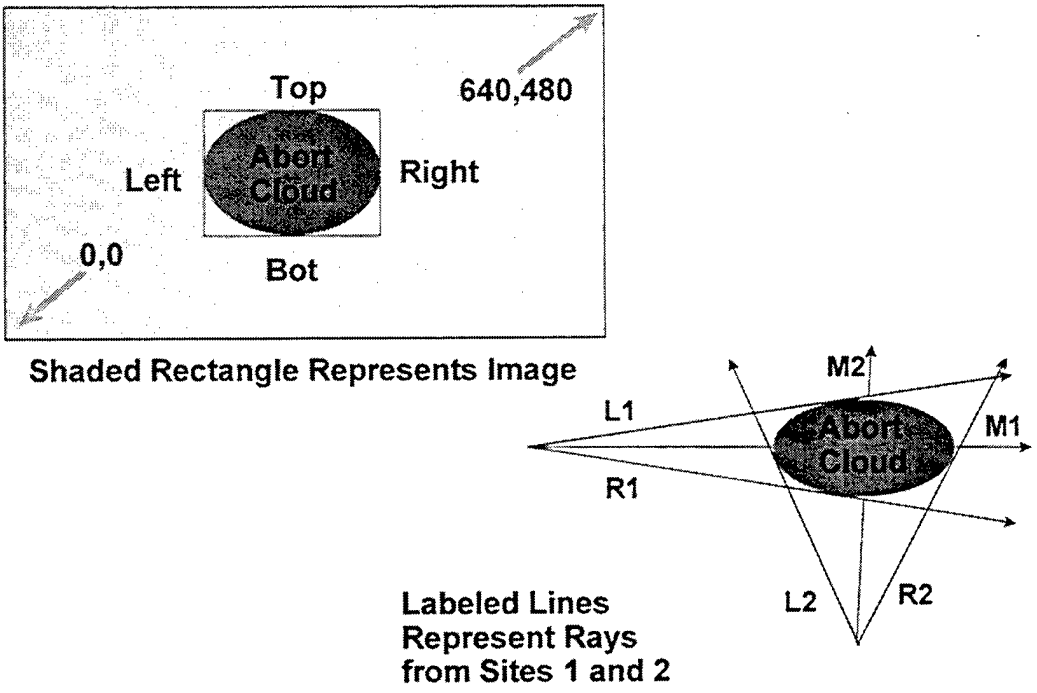


Figure 3. PLMTRACK box method and resulting rays.

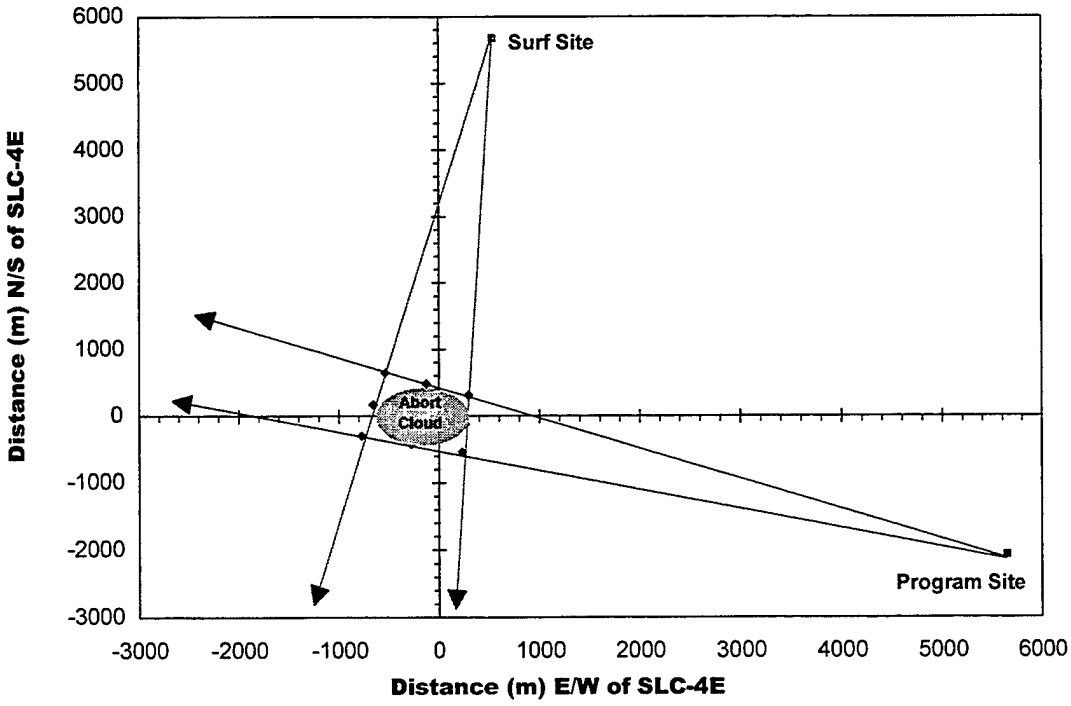


Figure 4. PLMTRACK ray tracing and extent of 34D-9 abort cloud at 78.378s.

coordinates for all "occupied" volume elements. The coordinates are relative to a reference (i.e., SLC-4E for x and y and mean sea level for z). PLMVOL calculates the total volume (i.e., sum of all occupied volume elements), the sphere-equivalent radius, and the mean altitude for the abort cloud (i.e., mean position of all occupied volume elements). For facile comparison to REEDM, this report uses altitude relative to SLC-4E pad rather than MSL in all plots.

The PLMVOL approach is illustrated by Figure 5 for simultaneous images of the Titan IV K-23 normal launch cloud from three sites. We used the K-23 images to illustrate PLMVOL since there were three sites and that cloud had a more complicated shape. The PLMVOL-derived reconstructed cloud is shown from a perspective similar to the middle image in Figure 5 but can be viewed from any perspective.

PLMVOL analysis of the Surf and Program imagery was possible between 37 and 78 seconds after the incident and documented that the abort cloud remained above SLC-4E. Indeed, there is excellent agreement between the PLMVOL, PLMTRACK, and single-site (i.e., Program and Surf analyzed independently) results. In addition to the ground track, the rise rate, and the extent that are also derived from PLMTRACK analysis, PLMVOL provided volumetric data that compares well with the single site ellipsoid estimates.

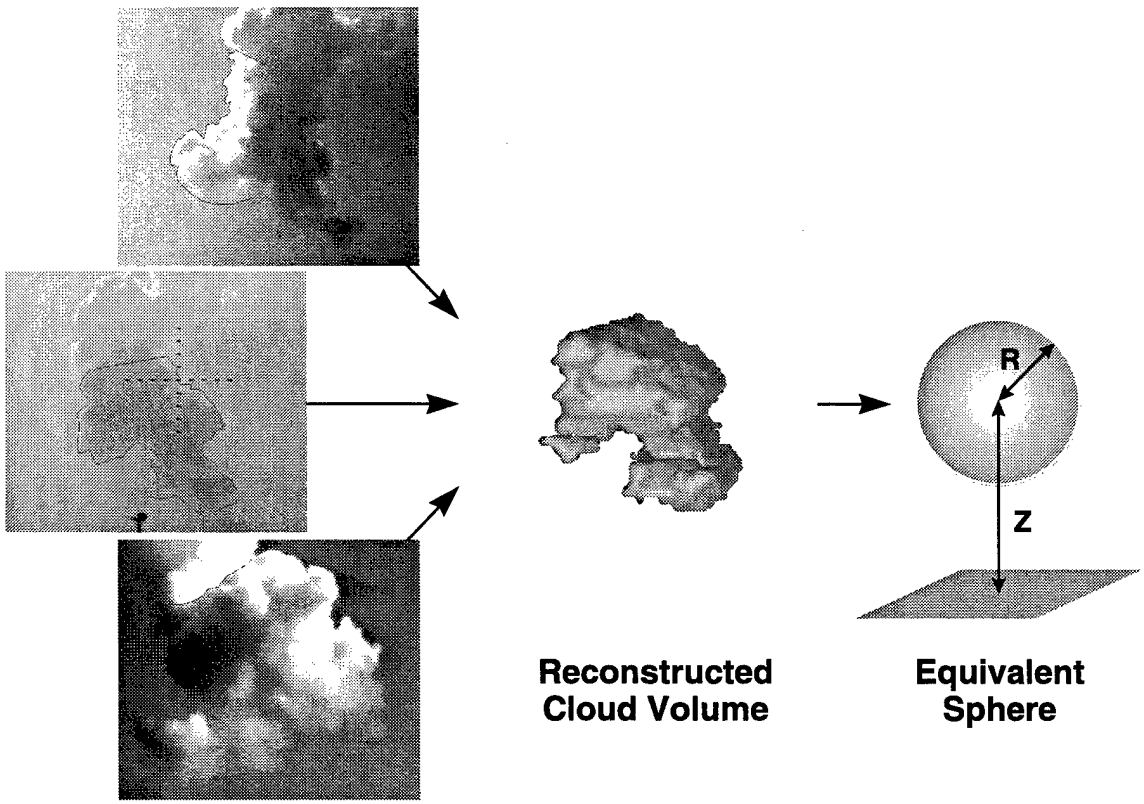


Figure 5. PLMVOL approach illustrated by Titan IV K-23 ground cloud images.

# 3. Results

The results of the quantitative analysis of the 34D-9 abort cloud imagery include calibration data, single-site analysis results, PLMTRACK results, and PLMVOL results. Each of these topics will be discussed in separate sections.

## 3.1 Calibration and Accuracy Information for Surf and Program Imagery

The primary calibration of the Surf site imagery used known landmarks that appeared in a single image. In contrast, the primary calibration of the Program site imagery used the known position of the moving Titan 34D-9 in a series of images. In both cases, the primary calibration allowed the secondary calibration of terrain features that were used to interpret subsequent images. The accuracy of the calibration was assessed by several methods. The analyst derived the altitude of the Titan 34D-9 vehicle from the calibrated images. This is obviously useful for the Surf site imagery since the primary calibration was by independent means (i.e., SLC-4E and SLC-4W in single image). For the Program site, the accuracy of the altitude profile for the Titan 34D-9 vehicle documented good secondary calibration. The primary calibration was based upon the height of the moving Titan 34D-9 vehicle as captured in a series of images from Program site. This sequence allowed the calculation of the AZ and EL to a secondary calibration landmark (i.e., a patch of sand on a hillside). Subsequently, this secondary calibration landmark was used to interpret Program site's imagery. As discussed in later sections, the PLMTRACK analysis indicated the accuracy of the imagery calibrations by its "projected" rays while the PLMVOL analysis indicated the accuracy of the imagery calibrations by the "reflected" images of the abort cloud. Both PLMTRACK and PLMVOL indicate good calibrations for the 34D-9 imagery.

Figure 6 is the primary calibration image for the Surf site. This single image contains both SLC-4E and SLC-4W. For calibration purposes, one can identify the mobile service towers (MST), the umbilical towers (UT), and the Titan 34D-9 vehicle. Therefore, one can calculate both the FOV and the pointing angle for each pixel in this image. Figure 6 and Figure 7 include several secondary calibration features that were used to calibrate subsequent images. The labels in Figure 6 and Figure 7 document the names (Patch 1, Patch 2, W1, W2, Pole) given to the various reference objects. Figure 6 also provides the X,Y pixel locations in the 640 by 480 pixel image for several primary and secondary references. We chose this resolution (i.e., 640 by 480) for digitizing the 34D-9 imagery and have archived these digitized images on optical disks.

Table 1 provides a listing of calibration information for Surf site imagery. For primary calibration references, Table 1 provides the latitude, longitude, and altitude of the references as well as its azimuth (AZsurf), elevation (ELsurf), and horizontal distance (Dsurf) relative to the Surf imagery site. In Table 1, Surf Site, the Launch Pad, and the Primary Calibration References (i.e., the Top of the Titan 34D-9 while on the Pad, Top Left of Umbilical Tower at SLC-4E, and SLC-4W Umbilical Tower) are presented in **bold letters**. The three remaining entries are secondary references and are at unknown absolute positions. Secondary references were identified in Figure 6 and in Figure 7. As discussed previously, the azimuth and elevation to the secondary references were interpreted from their pixel locations and from those of the primary references. The azimuth (AZsurf) and elevation (ELsurf) are to the reference object and from Surf site. The altitude in Table 1 is in meters relative to mean sea level (MSL). The distance is the horizontal distance between Surf site and the reference.

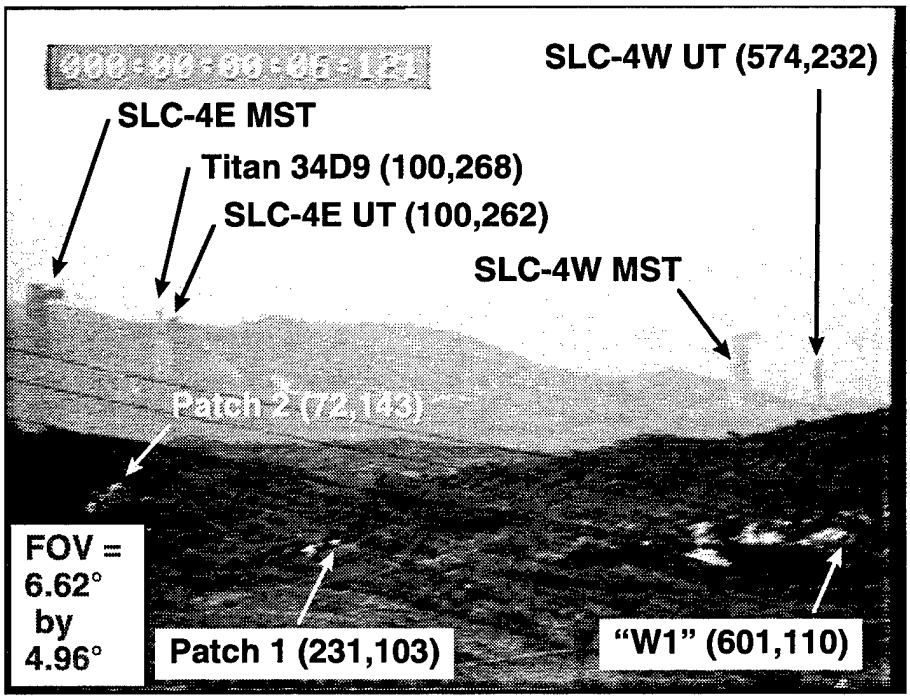


Figure 6. Primary calibration image for surf site.

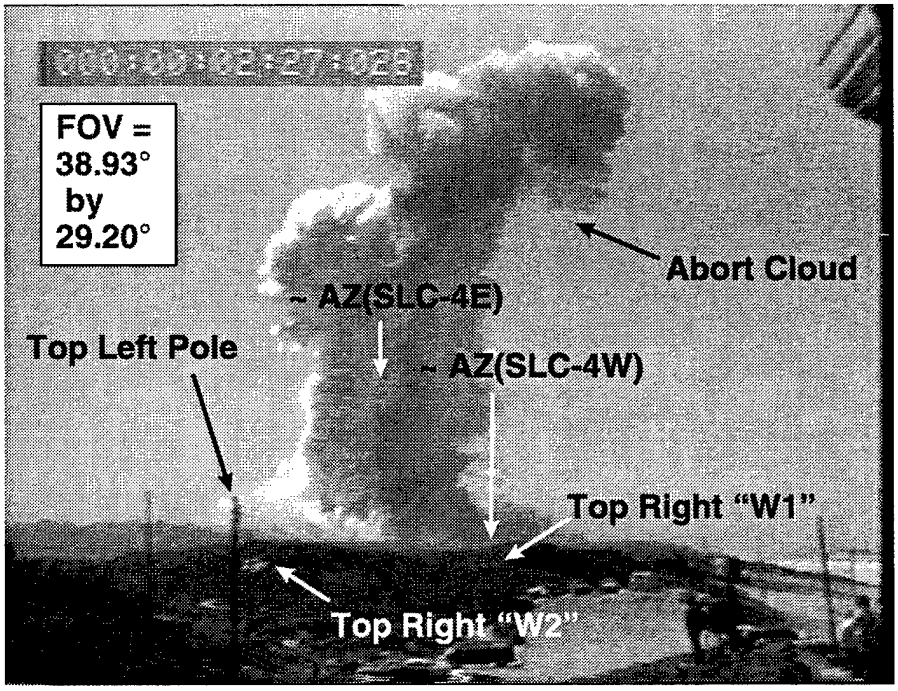


Figure 7. Secondary calibration image for surf site (T+129.83s after incident).

Table 1. Calibration Information for Surf Site.

| Reference | Latitude (Degrees) | Longitude (Degrees) | Alt (m MSL) | AZsurf (Degrees) | ELsurf (Degrees) | Dsurf (m) |
|---|---|---|---|---|---|---|
| **Surf Site** | **34.68307** | **-120.60477** | **62** | **#N/A** | **#N/A** | **0** |
| **SLC-4E Pad** | **34.63204** | **-120.61063** | **153** | **185.39** | **0.92** | **5706** |
| **Top 34D-9 Bird on SLC-4E Pad** | **34.63204** | **-120.61063** | **200** | **185.39** | **1.39** | **5706** |
| **Top Left UT at SLC-4E** | **34.63204** | **-120.61063** | **196** | **185.39** | **1.35** | **5706** |
| **SLC-4W Pad** | **34.63315** | **-120.6158** | **116** | **190.29** | **0.56** | **5648** |
| Top Left MST at SLC-4E | #N/A | #N/A | #N/A | 184.36 | 1.59 | #N/A |
| Top Right "W1" | #N/A | #N/A | #N/A | 190.56 | -0.23 | #N/A |
| Top Left "Pole" | #N/A | #N/A | #N/A | 178.93 | 2.82 | #N/A |

Figure 8 reveals the excellent accuracy of the Surf site calibration by comparing the imagery-derived altitude to the expected altitude for the Titan 34D-9 vehicle during the first 8 seconds of flight. In this report, altitude above ground level (AGL) is altitude above SLC-4E pad. Figure 9 documents the precision for Surf site measurements by plotting the percent difference in width (%(dW)) for objects observed in several FOVs. Since the FOV was used to interpret the width in each image, dW reflects the precision of the measurements. The FOV changed seven times during the 130 seconds of imagery. The precision of the width measurements for various secondary reference objects in all of these FOVs is approximately 4 percent. Figure 10 documents the magnitude of the FOV changes by documenting the relative size of objects in each of the FOVs relative to the object's size in FOV #1.

Figure 11 is one of the primary calibration images for Program site and shows the 34D-9 vehicle at 91 m (299 ft) above SLC-4E. This is the first of a series of images that contain both the secondary calibration reference and the 34D-9 vehicle prior to its abort. Therefore, one can calculate both the FOV and the pointing angle for this series of images if one assumes that the FOV did not change. This was verified to be a good assumption for Program site since the size of reference objects and the distances between reference objects did not change in these primary calibration images.

Table 2 provides a listing of calibration information for Program site imagery. For primary calibration references, Table 2 provides the latitude, longitude, and altitude of the references as well as its azimuth (AZprog), elevation (ELprog), and horizontal distance (Dprog) relative to the Program site. In Table 2, Program Site, the Launch Pad, and the Primary Calibration References (i.e., the bottom of the Titan 34D-9 while above Pad Hill and before the abort at T=0s) are presented in **bold letters**. The single remaining entry is the secondary reference and is at an unknown absolute position. The secondary reference was identified in Figure 11. As discussed previously, the azimuth and elevation to the secondary reference was interpreted from its pixel location and from those of the primary reference (i.e., the moving Titan 34D-9). The hill tops blocked the view of all launch facilities (i.e., the MSTs and UTs) from the Program perspective. The azimuth (AZprog) and elevation (ELprog) are to the reference object and relative to Program site. The altitude in Table 2 is

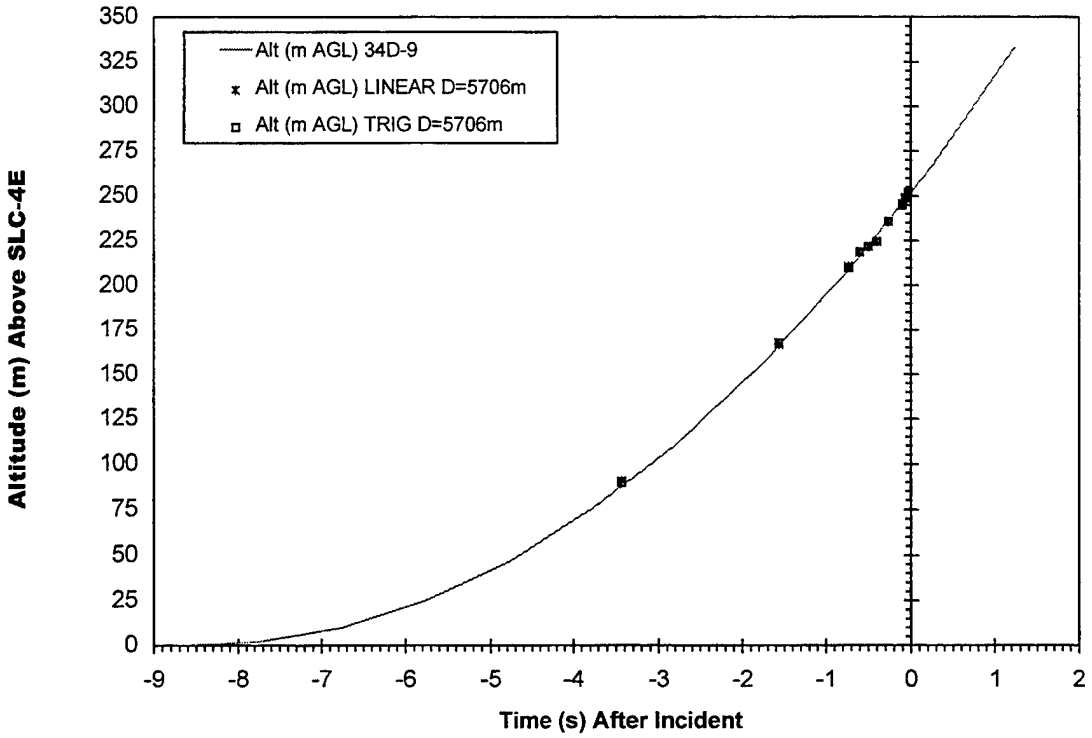


Figure 8. Surf site's imagery-derived versus actual Titan 34D-9 altitude.

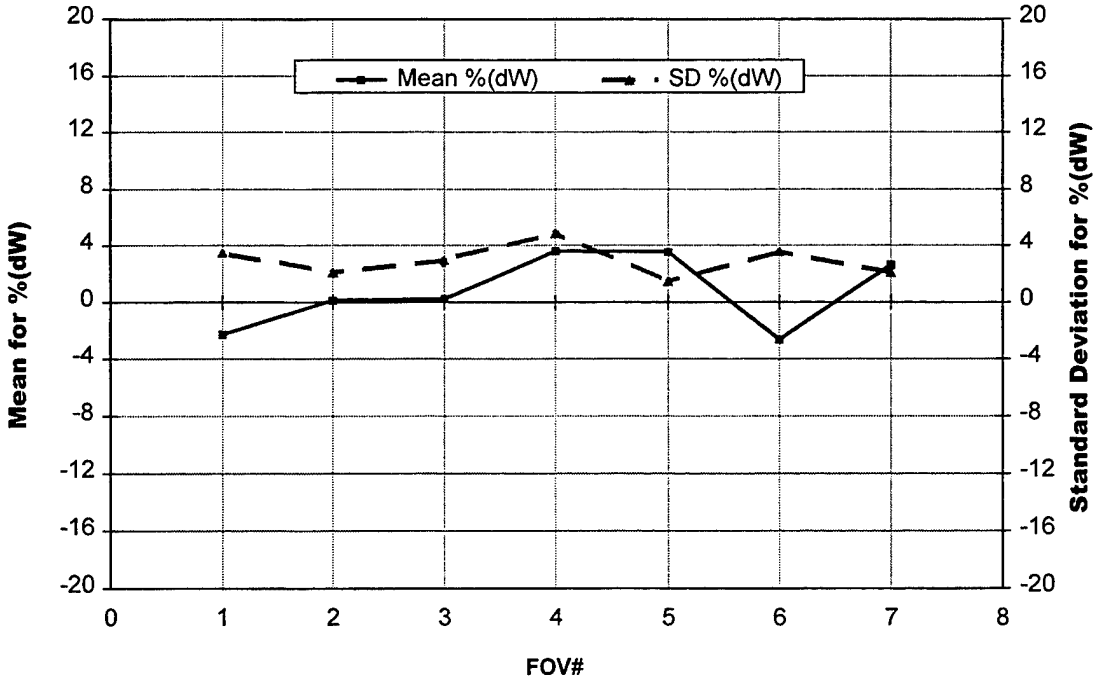


Figure 9. Precision estimates for the surf site imagery.

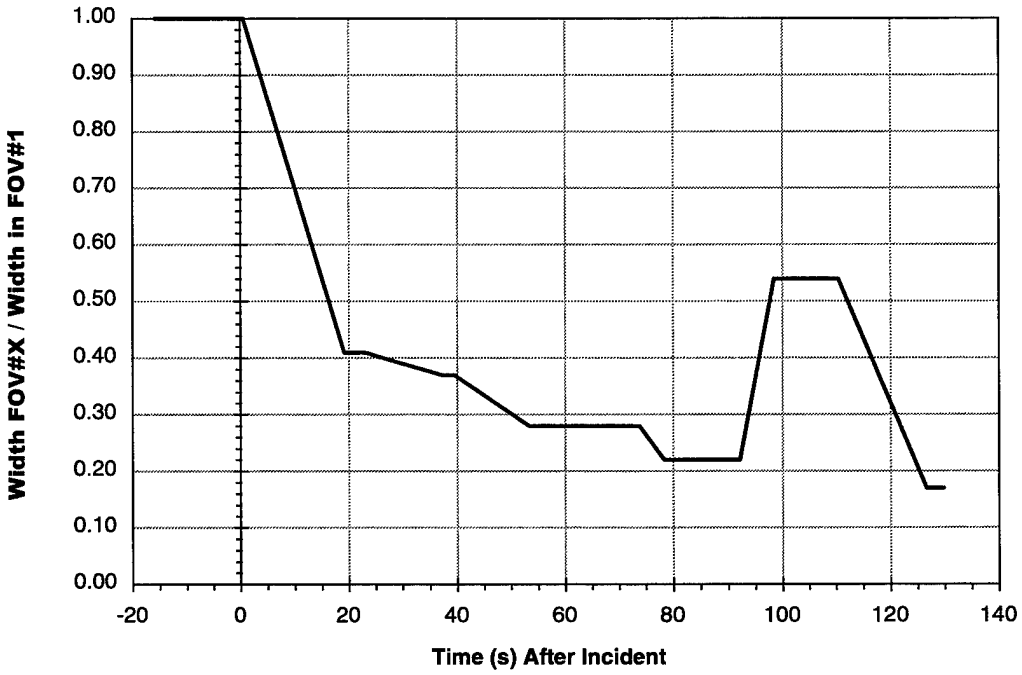


Figure 10. Relative size of objects in the various FOVs for surf imagery.

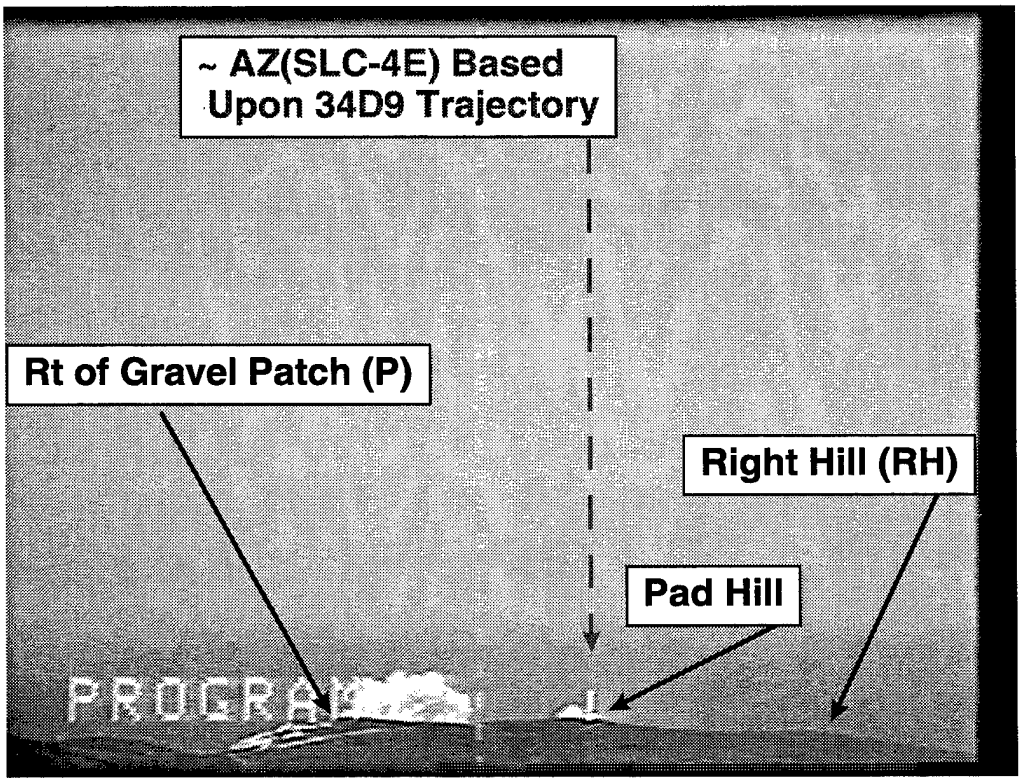


Figure 11. First of a series of primary calibration images for program site.

Table 2. Calibration Information for Program Site

| Reference | Latitude (Degrees) | Longitude (Degrees) | Alt (m MSL) | AZprog (Degrees) | ELprog (Degrees) | Dprog (m) |
|---|---|---|---|---|---|---|
| **Program Site** | **34.613430** | **-120.549025** | **393** | **#N/A** | **#N/A** | **0.00** |
| **SLC-4E Pad** | **34.632039** | **-120.610629** | **153** | **290.16** | **-2.29** | **6012** |
| **Bottom 34D-9 Bird at -3.437s** | **34.632039** | **-120.610629** | **244** | **290.16** | **-1.43** | **6012** |
| **Bottom 34D-9 Bird at -1.568s** | **34.632039** | **-120.610629** | **320** | **290.16** | **-0.70** | **6012** |
| **Bottom 34D-9 Bird at -0.734s** | **34.632039** | **-120.610629** | **364** | **290.16** | **-0.28** | **6012** |
| **Bottom 34D-9 Bird at -0.601s** | **34.632039** | **-120.610629** | **372** | **290.16** | **-0.21** | **6012** |
| **Bottom 34D-9 Bird at -0.501s** | **34.632039** | **-120.610629** | **375** | **290.16** | **-0.18** | **6012** |
| **Bottom 34D-9 Bird at -0.400s** | **34.632039** | **-120.610629** | **378** | **290.16** | **-0.15** | **6012** |
| **Bottom 34D-9 Bird at -0.267s** | **34.632039** | **-120.610629** | **389** | **290.16** | **-0.05** | **6012** |
| **Bottom 34D-9 Bird at -0.100s** | **34.632039** | **-120.610629** | **399** | **290.16** | **0.05** | **6012** |
| **Bottom 34D-9 Bird at -0.067s** | **34.632039** | **-120.610629** | **402** | **290.16** | **0.08** | **6012** |
| **Bottom 34D-9 Bird at -0.033s** | **34.632039** | **-120.610629** | **405** | **290.16** | **0.11** | **6012** |
| Right Top of Gravel Patch | **#N/A** | **#N/A** | **#N/A** | **287.35** | **-1.61** | **#N/A** |

in meters relative to mean sea level (MSL). The distance is the horizontal distance from Program site to the reference object (i.e., the Titan 34D-9 was directly above the SLC-4E pad).

Figure 12 reveals the accuracy of the Program site calibration by comparing the imagery-derived altitude to the expected altitude for the Titan 34D-9 vehicle during the first 8 seconds of flight. This analysis used the secondary reference to calibrate the image. Therefore, Figure 12 documents that the primary calibration was accurately transferred to the secondary reference. The FOV changed only three times for Program site imagery. As with the Surf site imagery, the FOV was determined by the relative size of objects in each image. Between 37s and 61s after the 34D-9 failure, objects were 0.57 their size in FOV #1. Between 73.774s and 78.378s after the 34D-9 failure, objects were 0.41 their size in FOV #1. The precision of the width measurements for various secondary reference objects in all of these FOVs was consistent with the pixel error for measuring the object size.

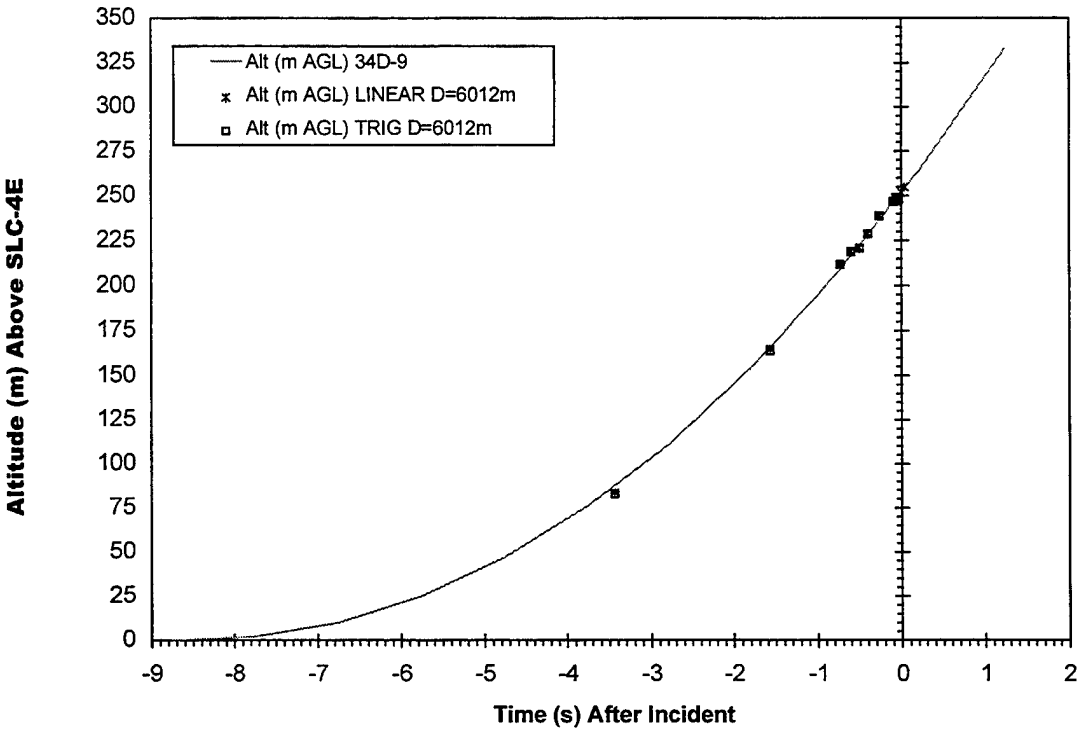


Figure 12. Program site's imagery-derived versus actual Titan 34D-9 altitude.

## 3.2 Single Site Analysis Results

This discussion is presented as two parts. First we will document the analysis of the Surf site's imagery using the reasonable assumption that the abort cloud remained over the pad. Second we will document the possible errors associated with this assumption and provide a refined estimate of the results based upon this error analysis. The available imagery and rawinsonde data suggest that there is a negligible error in assuming that the abort cloud remained over SLC-4E for the 130 seconds in question. Appendix D provides additional error analysis regarding the upward perspective. Those estimates suggest an error of only 5% for the entrainment coefficient.

### 3.2.1 The Abort Cloud Remained Over SLC-4E for the First 78 seconds

Figure 13 documents that the abort cloud remained over the launch pad for the first 78 seconds after the abort based upon Program site's imagery (i.e., an eastern perspective). Therefore, one can use the known distance between the launch pad and Surf site (i.e., a northern perspective) as the horizontal "ground" distance (i.e., D = 5706 m) for converting angular diameters and elevations (i.e., Figure 14) observed from Surf site to physical diameters and altitudes (i.e., Figure 15). In these figures, $d_{EW}$ is the horizontal diameter (i.e., in the east/west direction) and $d_V$ is the vertical diameter. The data in Figure 15 document linear increase in altitude and diameter between 20 and 130s after the 34D-9 failure. Extrapolation to T=0s gives 606m as the "initial" altitude for the cloud. This is substantially higher than the 252 m (827 feet) for the bottom of the 34D-9 at T=0s. Therefore, the initial fireball rose quickly to form the abort cloud at higher altitudes. Figure 15 illustrates that by 20s after the incident, the abort cloud had established a steady rate of rise and entrainment.

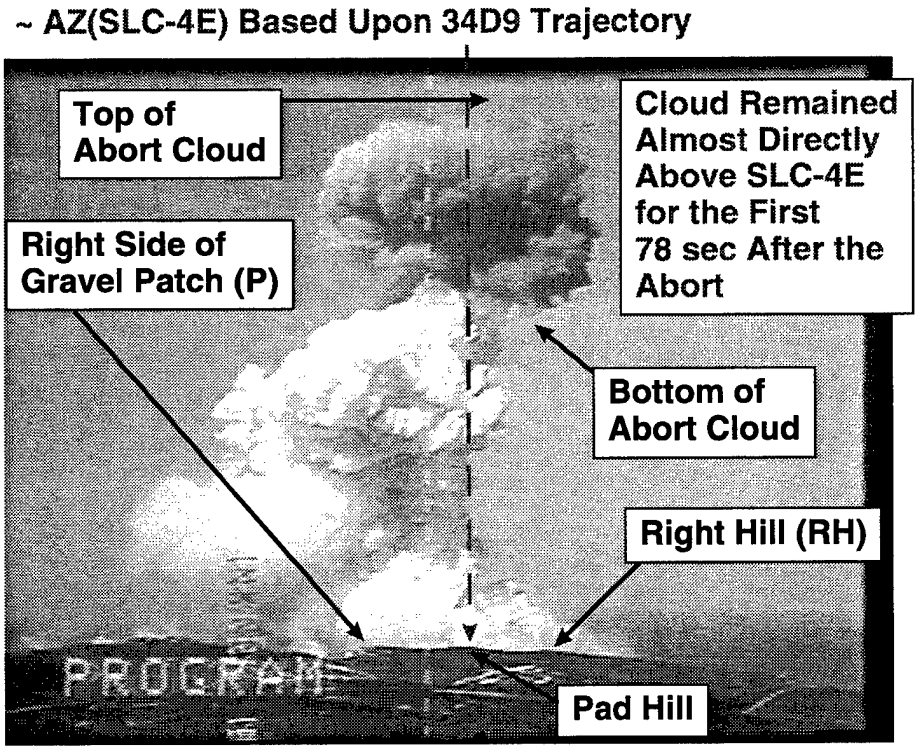


Figure 13. Abort cloud remained over SLC-4E from program perspective (T+78s).

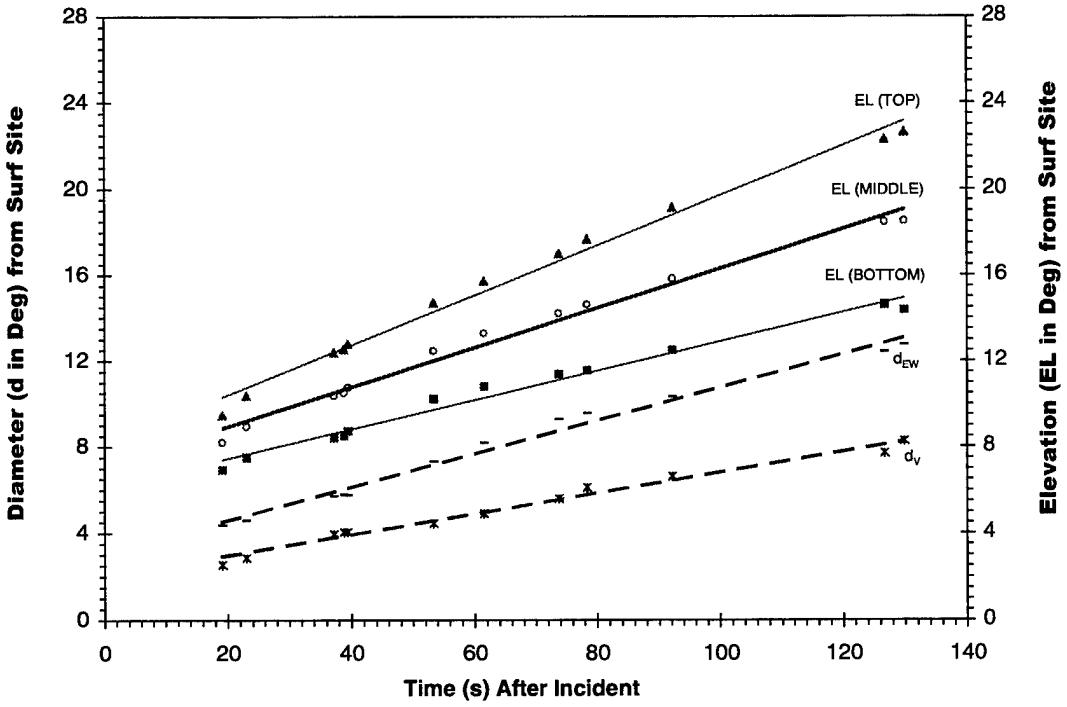


Figure 14. Angular abort cloud diameters and elevations from surf imagery.

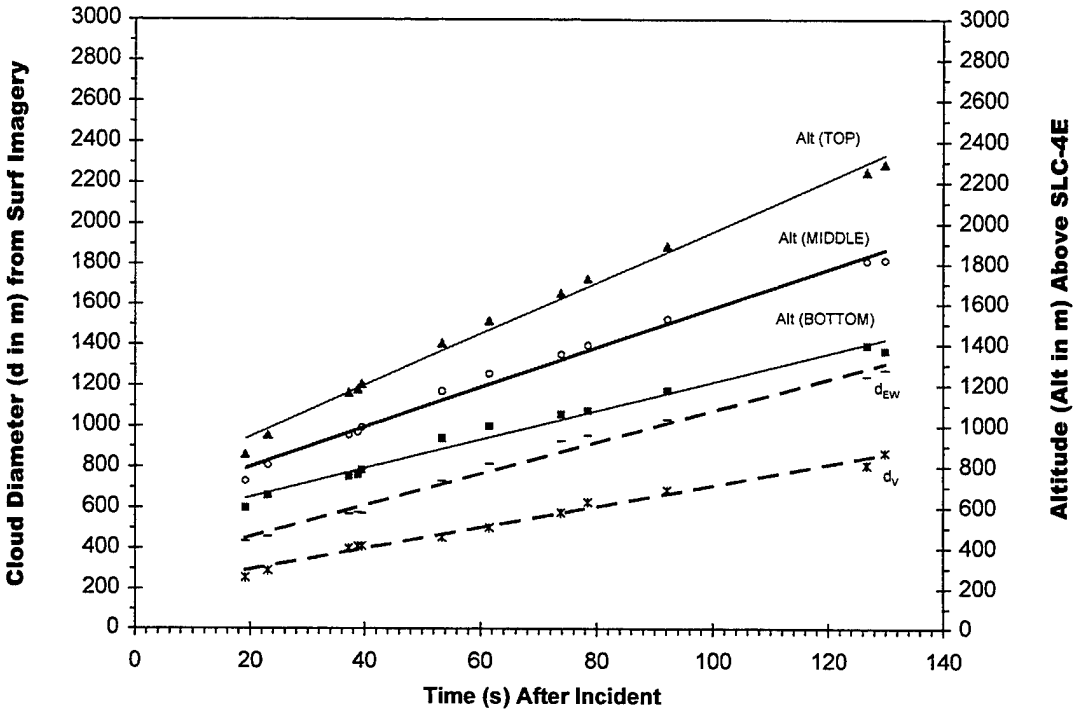


Figure 15. Physical abort cloud diameters and altitude by surf imagery (D=5706m).

Figure 16 is a time plot for the horizontal radius ($r_{EW}$ = radius along east/west axis) and vertical radius ($r_V$ = radius along vertical axis) of the abort cloud as derived from Surf imagery using D = 5706 m. Comparison reveals the obvious that these radii are half the diameters that were plotted in Figure 15. Figure 16 also includes the aspect ratio of the horizontal radius to vertical radius for the abort cloud as observed not only from Surf site (i.e., north of the abort cloud) but also from Program site (i.e., east of the abort cloud). The Surf-derived aspect ratios are represented by circles while the Program-derived aspect ratios are represented by asterisks. The solid line represents the average aspect ratio derived from the Surf data. It appears that, within the scatter of the data, the aspect ratio is equivalent for the east/west horizontal to vertical ratio (circles) observed from Surf site and for the north/south horizontal to vertical ratio (asterisks) observed from Program site. Therefore, one can approximate the volume of the abort cloud using the formula for an ellipsoid that has equivalent horizontal radii (i.e., $r_{EW} = r_{NS}$) and a smaller vertical radius ($r_V$). Figure 17 is a plot of the ellipsoid radii plotted in Figure 16 and the sphere equivalent radius against altitude. The sphere equivalent radius is derived from the following relationship:

$$r = \sqrt[3]{r_{EW} \times r_{NS} \times r_V} = \sqrt[3]{r_H^2 \times r_V}$$

where the east/west horizontal radius ($r_{EW}$) is set equal to the north/south horizontal radius ($r_{NS}$) in the second equation using the term $r_H$ to indicate a single value for both horizontal axes.

The above relationship resulted from the fact that the actual ellipsoid volume was set equal to the volume of a sphere to calculate the sphere-equivalent radius:

$$V_{ellipsoid} = \frac{4}{3} \times \pi \times r_{EW} \times r_{NS} \times r_V = \frac{4}{3} \times \pi \times r_H^2 \times r_V = V_{sphere} = \frac{4}{3} \times \pi \times r^3$$

The **slope (i.e., 0.35 in Figure 17)** of the line that fits a plot of the sphere-equivalent radius (r) against abort cloud altitude is, by definition, the **entrainment coefficient** used in the REEDM. The 34D-9 abort cloud's value of 0.35 (+/- 0.01) is equivalent to the values measured by quantitative imagery for several normal Titan IV launches (i.e., K-23, K-19, and K-24) from CCAS. REEDM uses a default value of 0.64 for the entrainment coefficient. Appendix D provides the error analysis for the upward perspective from Surf site.

The formula (i.e., r = 0.35 x Alt - 82.57) for the fit to the sphere-equivalent radius (r) plotted against altitude can be used to estimate the initial radius of the abort cloud. The data in Figure 15 documented a linear increase in altitude between 20 and 130s after the 34D-9 failure. As mentioned previously, extrapolation to T=0s gives 606m as the "initial" altitude for the middle of the cloud. Substitution of this value into the formula for the radius versus altitude yields an initial radius of 130m which is 10% larger than REEDM's value of 118m. In Figure 16, extrapolation of $r_V$ and $r_{EW}$ to T=0 gives initial vertical and horizontal ellipsoid radii of 95 and 150m, respectively. These values for the ellipsoid radii convert to a 129m sphere-equivalent radius which, as expected, is consistent with the extrapolated sphere-equivalent radius.

Figure 18 is the plot of the abort cloud's ellipsoid volume versus time. The volume data between 37 and 78 seconds should be comparable to the PLMVOL results presented in a later section. This comparison reveals that the ellipsoid volume estimates based upon separate analysis of the Surf imagery are comparable to the volume of the intersecting rays derived from simultaneous imagery from two sites. Therefore, it appears that the single-site analysis provides a useful estimate of cloud volume at these early times.

### 3.2.2 Estimates for Times Greater than 78 seconds

The data plotted in Figure 15 through Figure 18 were derived from Surf imagery assuming that the horizontal distance (*D*) between the center of the abort cloud and Surf site was 5706 m (i.e., the abort cloud remains directly over SLC-4E). Program site's imagery documents that the cloud was very slightly (i.e., 1/22 of its' horizontal diameter in Figure 13) to the south of SLC-4E by 78 seconds after launch. One can estimate the ground distance (*D*) between surf site and the center of the abort cloud from the diameters (d) of the abort cloud in Figure 13 using the following approximations:

$d_{EW}$ at 78 seconds ~ 950m

$d_V$ at 78 seconds ~ 600m

Center of Cloud = 1/22 * 950m to South of SLC-4E therefore *D*= 5749m

therefore corrected $d_{EW}$ = 950 * 5749/5706 = 957 m (0.75% larger)

and corrected $d_V$ = 600 * 5749/5706 = 605 m (0.75% larger)

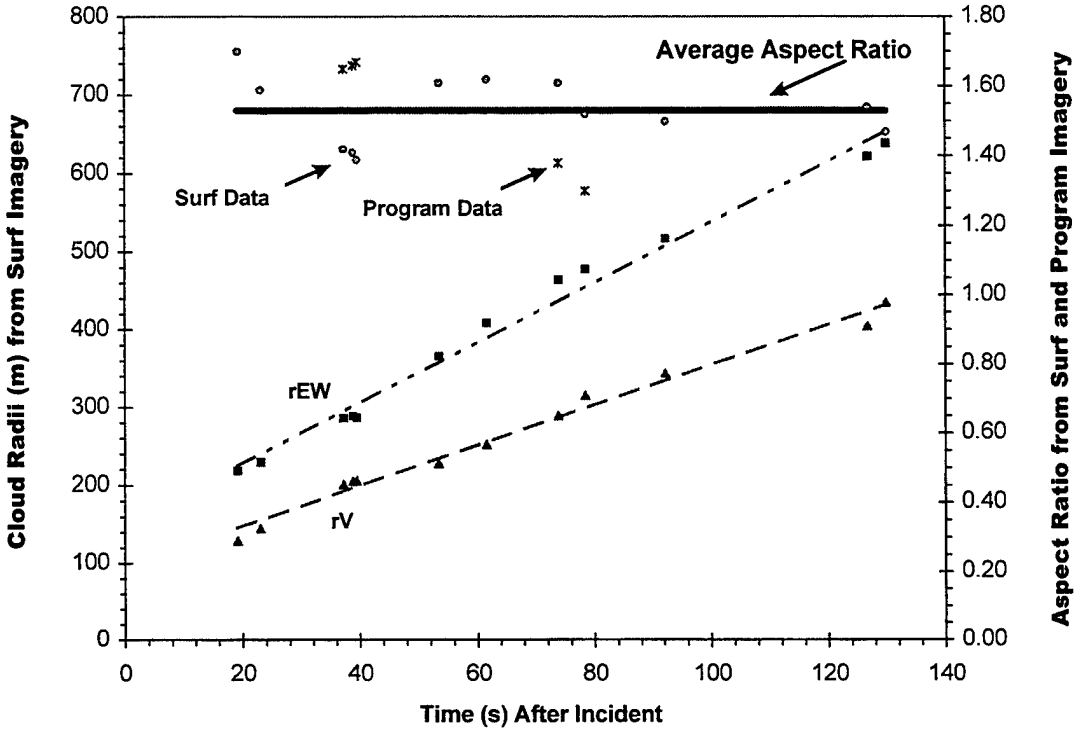


Figure 16. Abort cloud horizontal to vertical aspect ratios derived from both sites.

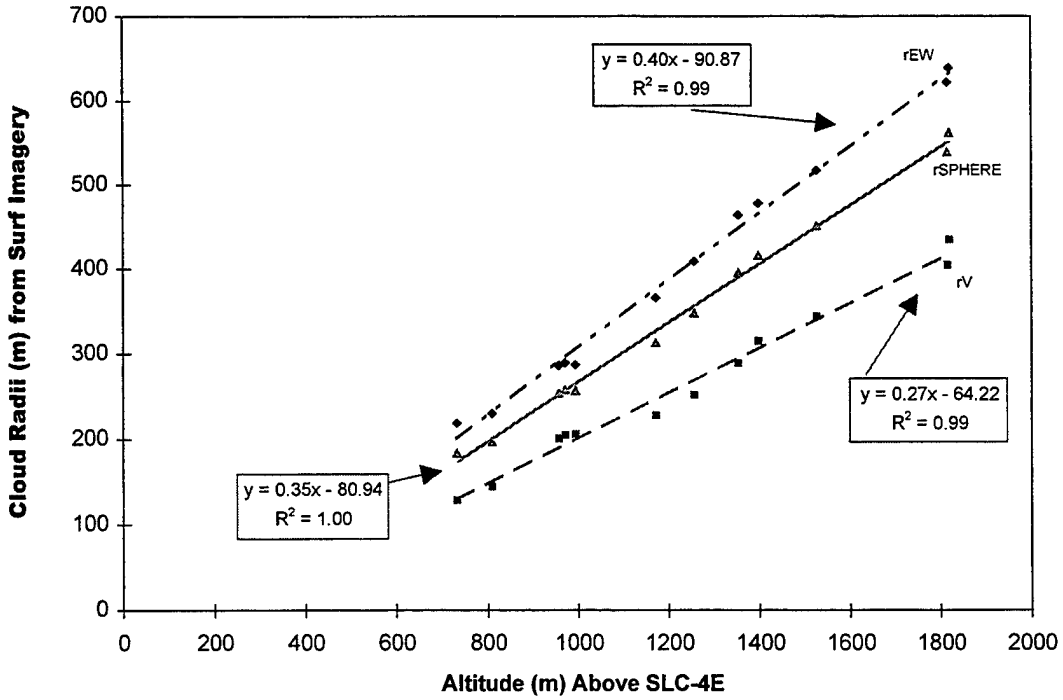


Figure 17. Ellipsoid radii and sphere equivalent radii based upon surf imagery.

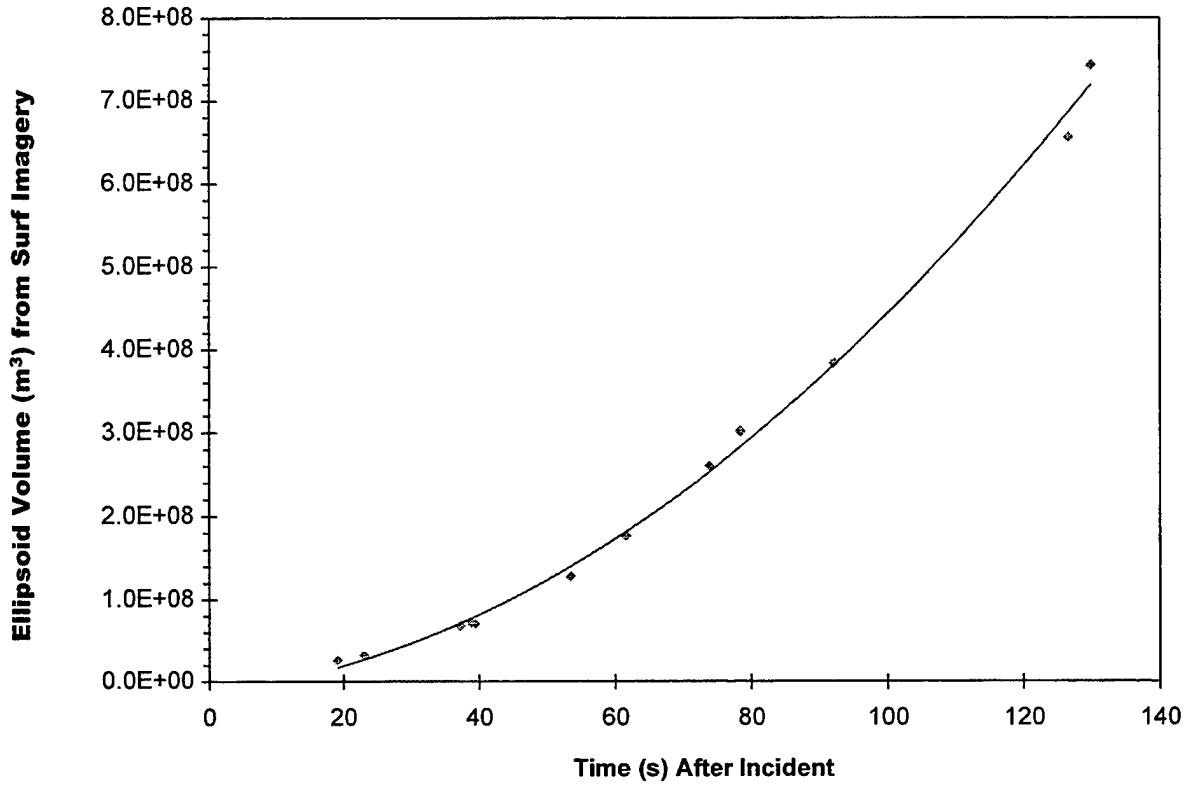


Figure 18. Ellipsoid volume versus time plot derived from surf site's imagery.

Between 80 and 129 seconds, the cloud should move with the wind as measured between 1380 and 2052 m AGL by the 18:15 GMT Rawinsonde (i.e., T-0.5 hour). We will use this approximation to estimate the magnitude of errors associated with the single site assumption (i.e., no lateral movement for the first 130 seconds after the 34D-9 failure).

Table 3 documents the magnitudes of the corrections (i.e., "Shift") for the ground distance (*D*) based upon Program imagery at 78 seconds after the abort and upon the rawinsonde winds at later times. The altitudes in Table 3 are based upon the imagery-derived altitude for the middle of the abort cloud at various times after the abort. This analysis will show that the imagery-derived abort cloud diameters and altitudes are not significantly affected by these corrections. Table 3 provides the direction and speed for the wind from the rawinsonde data. "v(Surf)" is the component of wind speed directed towards Surf site (i.e., northern component). The "Time" in Table 3 is relative to the failure event. "Shift" is the integrated change in distance while "Dsurf" is the corrected horizontal distance between Surf site and the abort cloud. The "Error" expresses the "Shift" as a percentage of the value of D (i.e., 5706 m) used in the uncorrected analysis. Apparently there is less than a 3% error in using the uncorrected value of D for the 130 seconds of available imagery.

Figure 19 is the "corrected" version of Figure 17 where the abort cloud radii and the sphere-equivalent radius were plotted against the abort cloud's altitude. The "corrected" values of *D* (i.e., Dsurf in Table 3) were used to calculate the results plotted in Figure 19. It is apparent that the slopes and, therefore, the entrainment coefficient (i.e., 0.35) were not affected by the relatively minor

Table 3. Ground Distance Estimates Based upon Program Imagery and Rawinsonde Winds

| Altitude (m AGL) | Direction (Degrees) | Speed (m/s) | v(Surf) (m/s) | Time (s) | Shift (m) | Dsurf (m) | Error (% of D) |
|---|---|---|---|---|---|---|---|
| Imagery | Wind | Wind | Wind | 80 | +043 | 5749 | +0.75 |
| 1380 | 122 | 6.69 | 3.55 | 80 | -007 | 5699 | -0.12 |
| 1521 | 125 | 7.2 | 4.13 | 94 | -127 | 5579 | -2.23 |
| 1793 | 132 | 5.14 | 3.44 | 123 | -151 | 5555 | -2.65 |
| 2052 | 141 | 1.54 | 1.2 | >130 | | | |

changes from the assumed ground distance (D=5706 m). Therefore, the assumption that *D* was approximately equal to the distance between the imagery site and SLC-4E was adequate for this data.

### 3.3 PLMTRACK Analysis Results

PLMTRACK provides an indication of the accuracy of the imagery calibrations by "projecting" a ray from a selected pixel in an image from one site into the sister image from the other imagery site. Figure 20 illustrates such a projection by indicating a pixel (+) in the Surf image and a projection of that ray (line) into the Program image. The projected ray hits the top of the cloud in the Program image at a reasonable position on the abort cloud and thereby documents good calibration information for this pair of images. This projected ray also illustrates that Surf imagery has a low elevation angle for viewing the abort cloud. This is important since a steep lookup angle could overshoot the top of the cloud. For a steep lookup angle, the analyst would not be able to see the top of the cloud because the edge of the cloud would block his view. This does not appear to be the case for the 34D-9 abort imagery. Appendix D provides error analysis for the worst-case lookup perspective for the actual 34D-9 imagery from Surf site.

Figure 21 and Figure 22 document the boxes used for PLMTRACK analysis of the T+37.204s and T+78.378s image pairs, respectively. These images represent the earliest and latest images that have simultaneous views from Program and Surf sites (left and right images, respectively). The times are relative to the abort incident. It is apparent that the boxes touch the top, left, right, and bottom extremes of the abort cloud in each of the perspectives. As discussed previously, the nearest approach of rays derived from such boxes document the three dimensional position of the abort cloud and its extent (Figure 4).

Figure 23 is a plot of the Cartesian coordinates for the two imagery sites and for the middle of the abort cloud derived from PLMTRACK analysis of the paired images from Surf and Program sites. The Cartesian plot is centered on SLC-4E (i.e., at 0,0 coordinates) and is scaled to include the

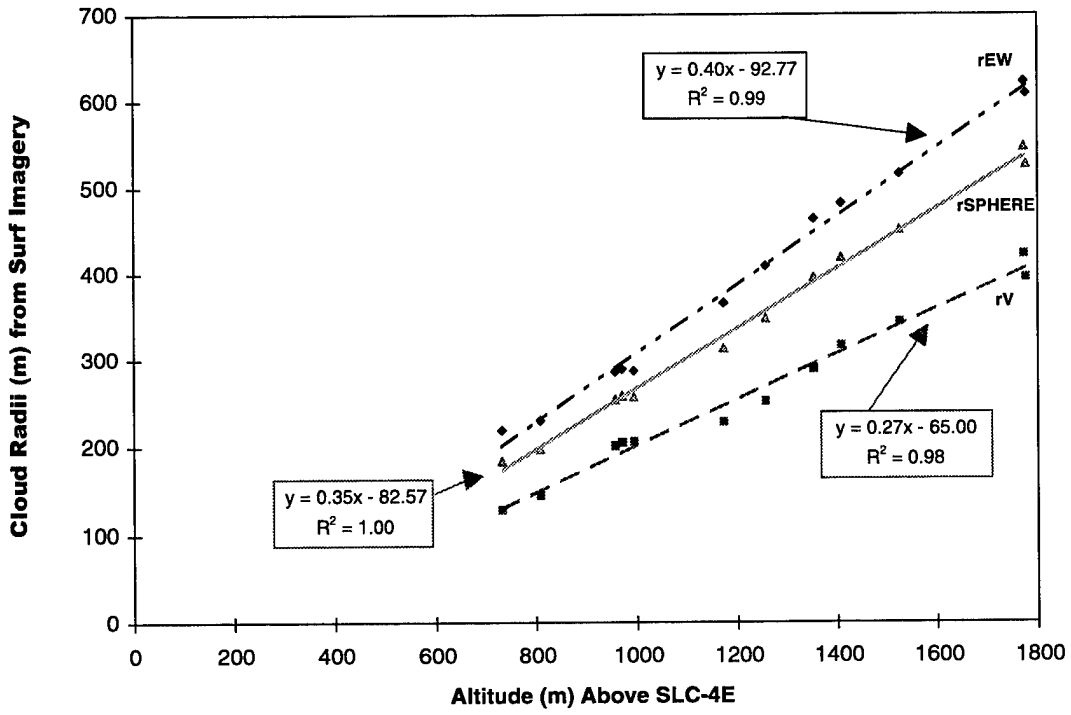


Figure 19. Entrainment data for surf site based upon corrected ground distances.

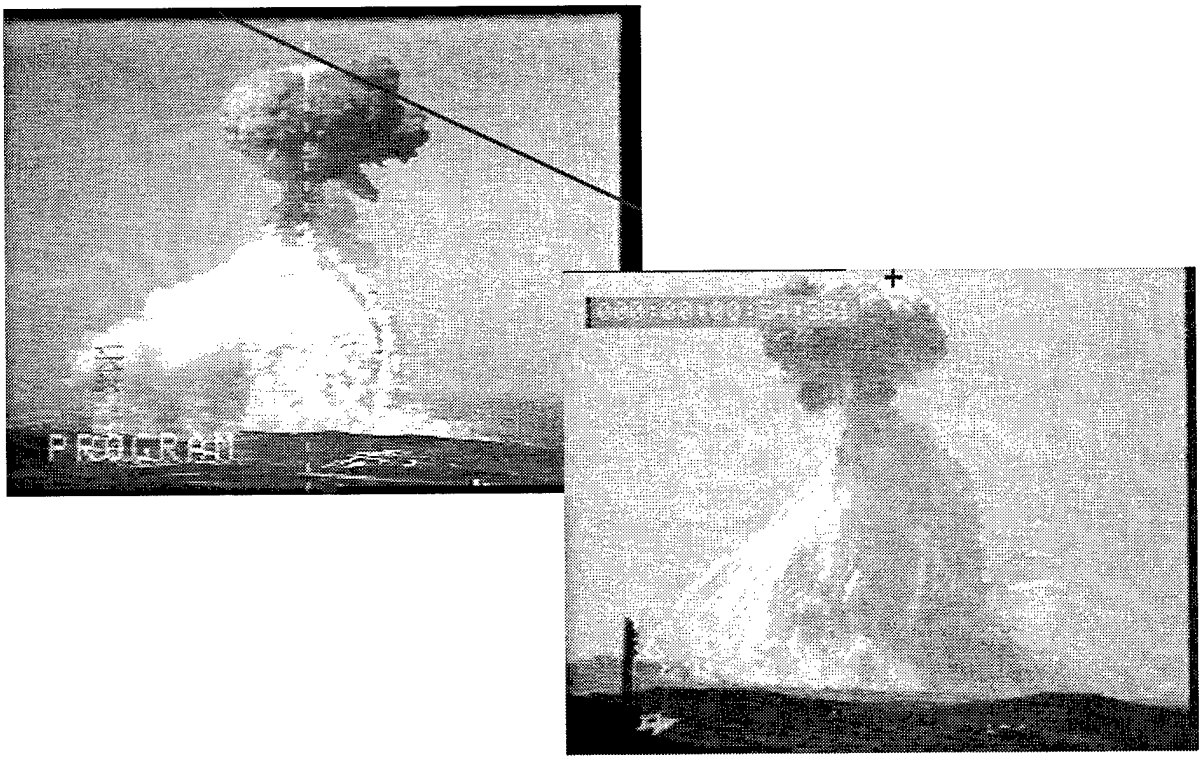

Figure 20. Projected ray in program image from pixel in surf image (T+37.204s).

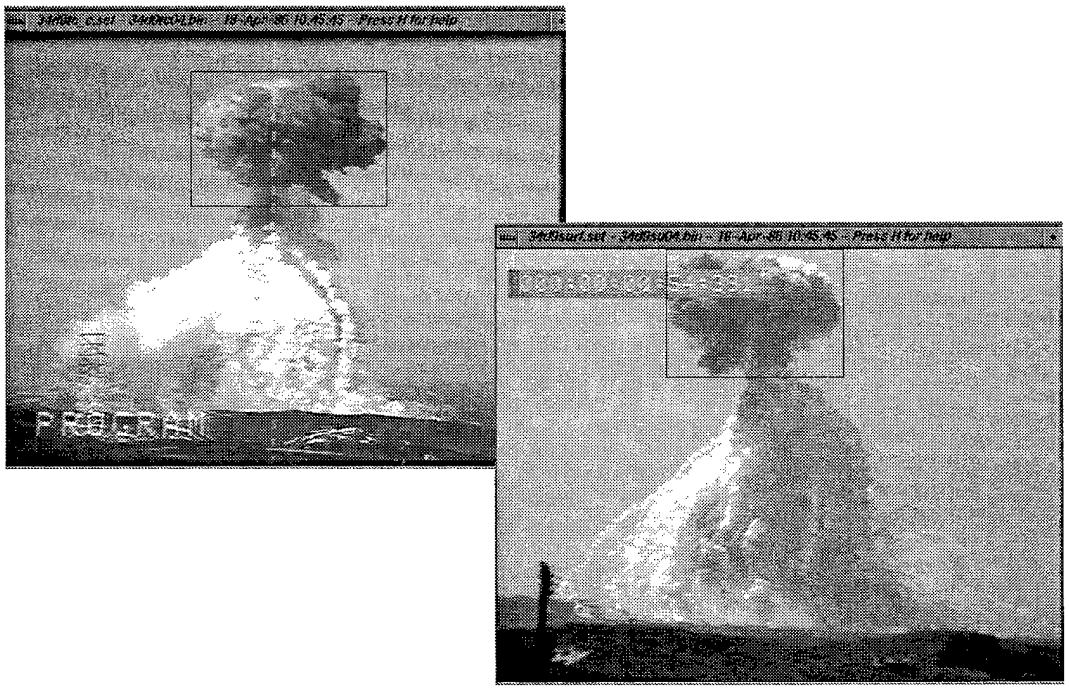

Figure 21. PLMTRACK boxes about abort cloud in program and surf images (T+37.204s).

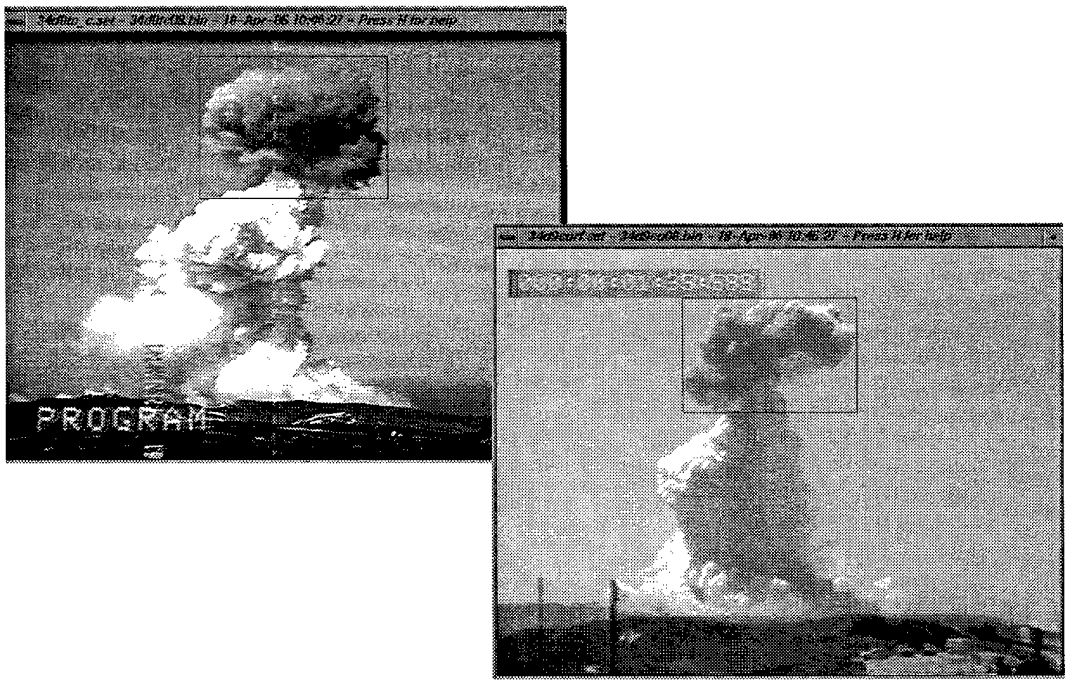

Figure 22. PLMTRACK boxes about abort cloud in program and surf images (T+78.378s).

coordinates for both Surf and Program sites (i.e., see the labeled symbols). It is apparent from Figure 23 that the middle of the cloud remained near the pad and that the ground distance between Surf site and the middle of the abort cloud remained essentially constant during the first 78s after the failure event. The dual-site PLMTRACK results are so closely packed that they appear to be only two points. In reality, there are two clusters of data: one for imagery near 37 seconds and the second for imagery near 78 seconds after the event. The middle of the cloud moved slightly to the northwest according to this plot.

Figure 24 documents the rise of the top, middle, and bottom of the abort cloud during the 130 seconds of Surf imagery. The hollow symbols represent altitudes estimated using only the Surf imagery and assuming that the abort cloud remained above the pad. The filled symbols represent the PLMTRACK results that were obtained by using pairs of images from both Surf and Program sites and without making any assumptions about the abort cloud. There is excellent agreement between the hollow (i.e., single site) and filled (i.e., PLMTRACK) results. Therefore, the assumptions used in processing the Surf imagery seem reasonable based upon this comparison.

## 3.4 PLMVOL Analysis Results

PLMVOL analysis requires simultaneous imagery from two (or more) imagery sites. The analyst draws an outline about the abort cloud in the image from each of the sites as illustrated in Figure 25 for the T+37.204s images from Program and Surf sites. PLMVOL then fills the outlines (i.e., Figure 26 for T+37.204s images) indicating the identification of all pixels contained within each outline. From these pixels, PLMVOL projects rays into space and determines all volume elements that are intersected by abort cloud rays derived from all available sites. Lastly, PLMVOL indicates the accuracy of the imagery calibrations by its "reflected" images of the abort cloud which ideally fills the original outlines in each of the images. Figure 27 shows the reflected abort cloud volume elements as blue dots (i.e., dark highlighting for black and white hardcopy) within the original outlines for the T+37.204s image pair. Figure 28 is a similar reflected abort cloud image pair for T+78.378s which was the last image pair available for Program and Surf sites. The reflected abort cloud images nearly fill the original outlines as illustrated by these figures. The fill is complete for the Surf images while accounting for most of the abort cloud as seen from Program site. These results suggest reasonably good calibration for the Program imagery. The unfilled lobe in the Program perspective accounts for less than ten percent of the total area.

PLMVOL analysis results in a listing of the x,y,z coordinates for all abort cloud volume elements based upon by rays from both imagery sites. Figure 29 is a plot of the altitudes for the top, middle, and bottom of the abort cloud against time after the failure incident. Paired imagery was only available for a few seconds about 37 and 78 seconds after the abort. The filled shapes in Figure 29 represent PLMVOL results: the highest altitude of any volume element, the mean altitude for all volume elements, and the lowest altitude of any volume element. The hollow shapes in Figure 29 represent single-site analysis results: the top, the middle, and the bottom altitude based upon the elevations observed from Surf site and the assumption that the cloud remained over the pad. Figure 29 documents excellent agreement between the two methods in spite of the differences between the "mean" and the "middle." The mean is the weighted average altitude. The middle is the average of the top and bottom. For unsymmetrical shapes, the mean would differ from the middle.

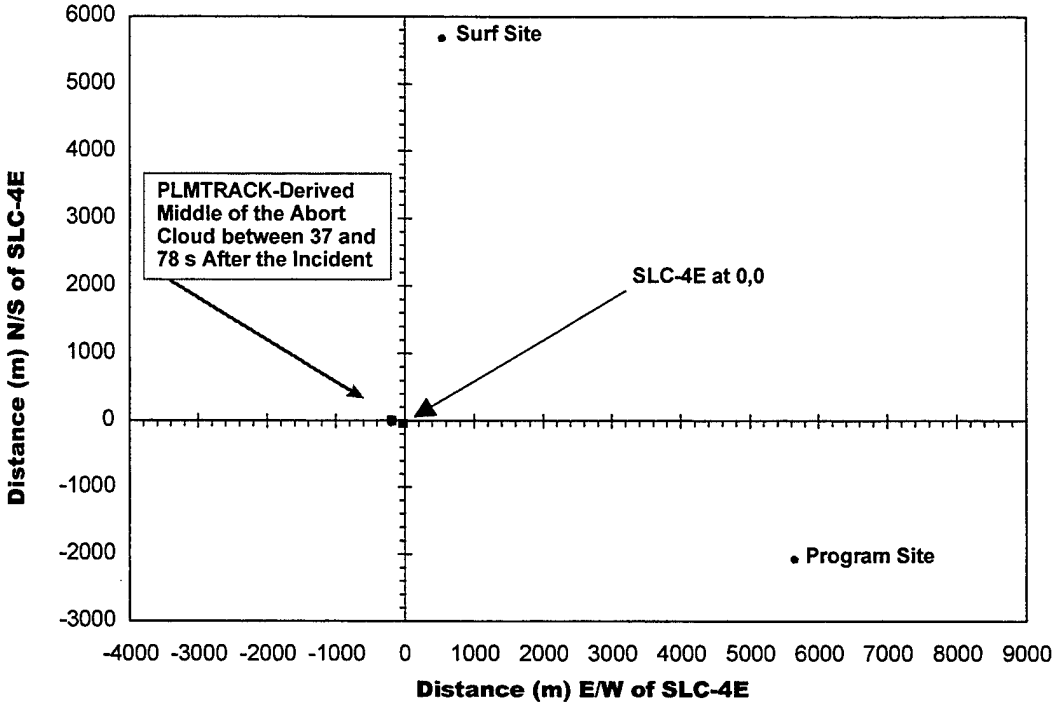


Figure 23. Abort cloud Cartesian coordinates derived by PLMTRACK analysis (37 to 78s).

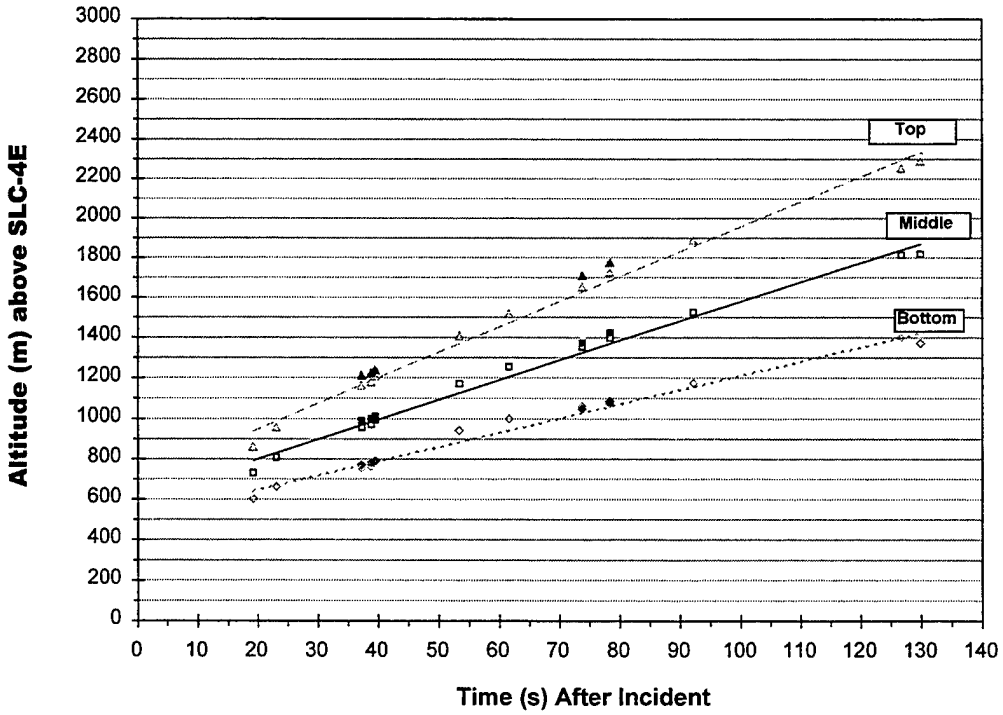


Figure 24. Cloud rise plots: PLMTRACK (filled) versus surf only (hollow) results.

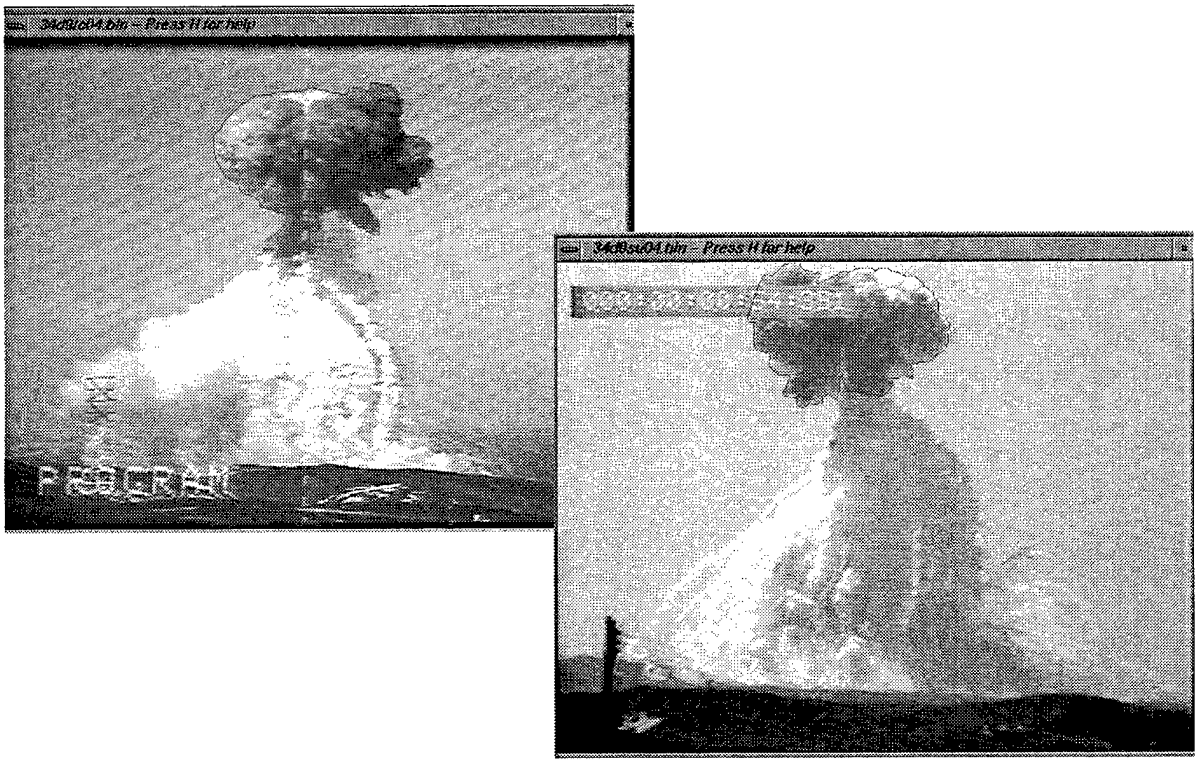

Figure 25. PLMVOL "outlines" for program and surf imagery (T+37.204s).

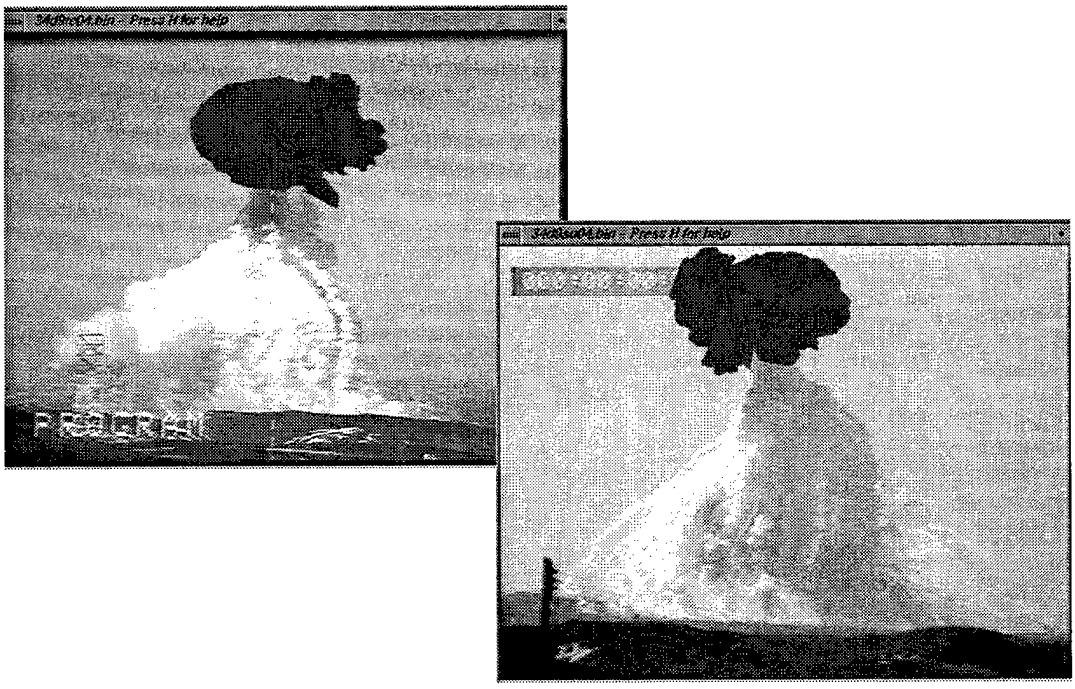

Figure 26. PLMVOL "fill" of outlines for program and surf imagery (T+37.204s).

Figure 27. PLMVOL "reflection" of abort cloud volume elements (T+37.204s).

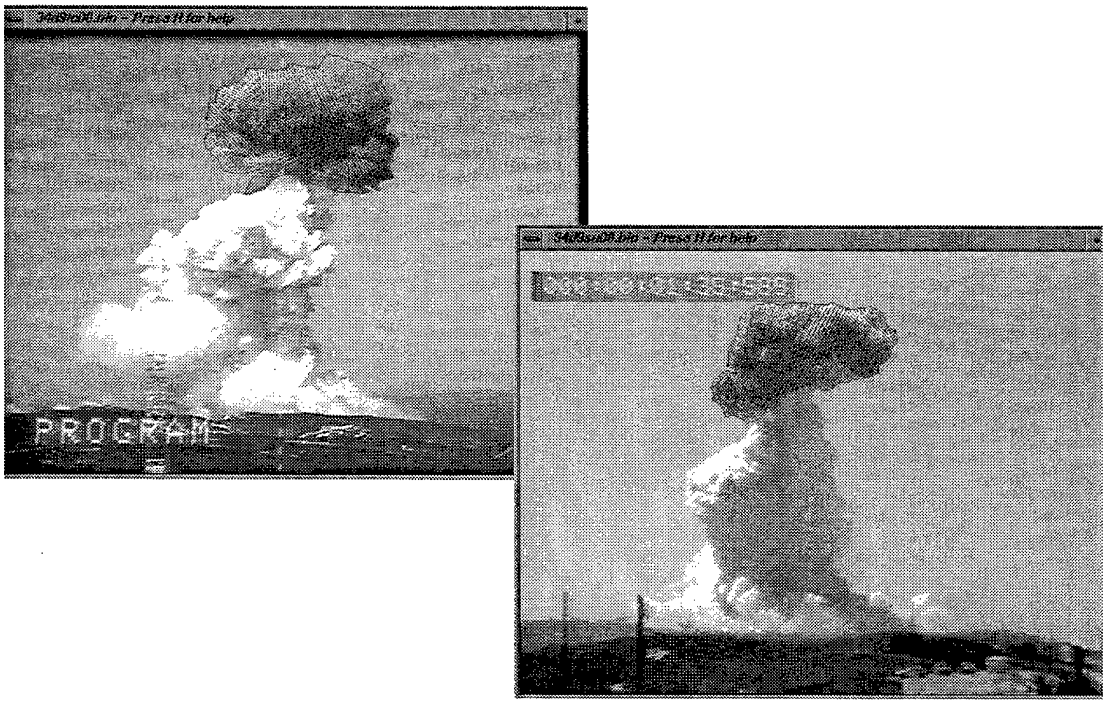

Figure 28. PLMVOL "reflection" of abort cloud volume elements (T+78.378s).

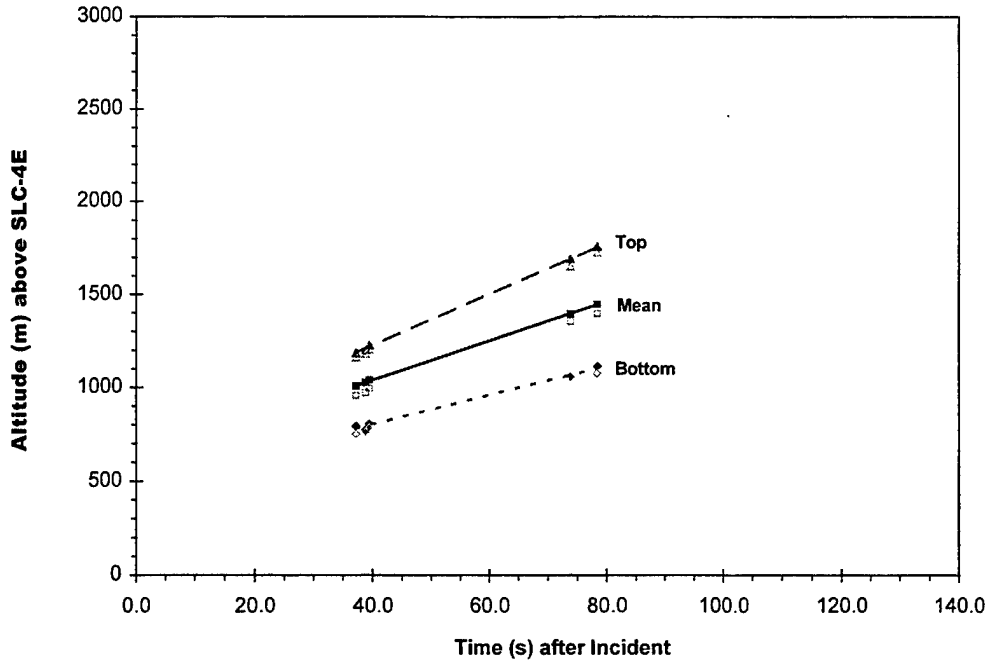


Figure 29. Abort cloud rise plots: PLMVOL(filled) versus surf only (hollow) (37 to 78s).

Figure 30 is the projected Cartesian extent of the abort cloud at T+78.378s after the incident based upon the PLMVOL-derived x,y coordinates of intersected abort cloud volume elements. It is similar to PLMTRACK's extent as documented in Figure 4 for the same images. Volume elements at different altitudes were assigned different colors (i.e., shades of gray in hardcopy) in Figure 30 to illustrate that the bottom, middle, and top of the cloud had different extents as derived by the PLMVOL analysis. Figure 31 is the Cartesian plot of the mean abort cloud position derived by PLMVOL for the available dual-site imagery. This plot is formatted identically to Figure 23 that presented similar PLMTRACK Cartesian results. Like that figure, the coordinates are relative to SLC-4E (i.e., 0,0) and are scaled to include both Surf and Program sites. Both the PLMVOL and the PLMTRACK analyses validate the assumption that the cloud remained about the same distance from Surf site for the first 78s after the abort. The cloud moved slightly to the west by 78s after the abort.

PLMVOL calculated the abort cloud's volume by summing all included volume elements and calculated the sphere-equivalent radius from that total volume. Figure 32 plots the PLMVOL results for volume and sphere-equivalent radius against altitude above SLC-4E. As mentioned previously, the slope of the plot of sphere-equivalent radius against altitude is defined as the entrainment coefficient. For comparison purposes, Figure 33 is a plot of the sphere-equivalent radius against altitude above SLC-4E and includes not only the PLMVOL results but also those from single-site analyses of the Program and Surf imagery. It is apparent that the PLMVOL values fall between the Program and Surf values at low altitudes and that the three methods give identical values at the higher altitudes. It appears that the Surf and PLMVOL results are within error bars at all altitudes.

Due to the limited altitude range sampled by the PLMVOL method and by the Program imagery, the best estimate (i.e., 0.35) for the entrainment coefficient is from Figure 19. The Surf data plotted in

Figure 19 cover altitudes from 700 to 1750 m rather than the limited 950 to 1450 m covered by the PLMVOL data in Figure 33.

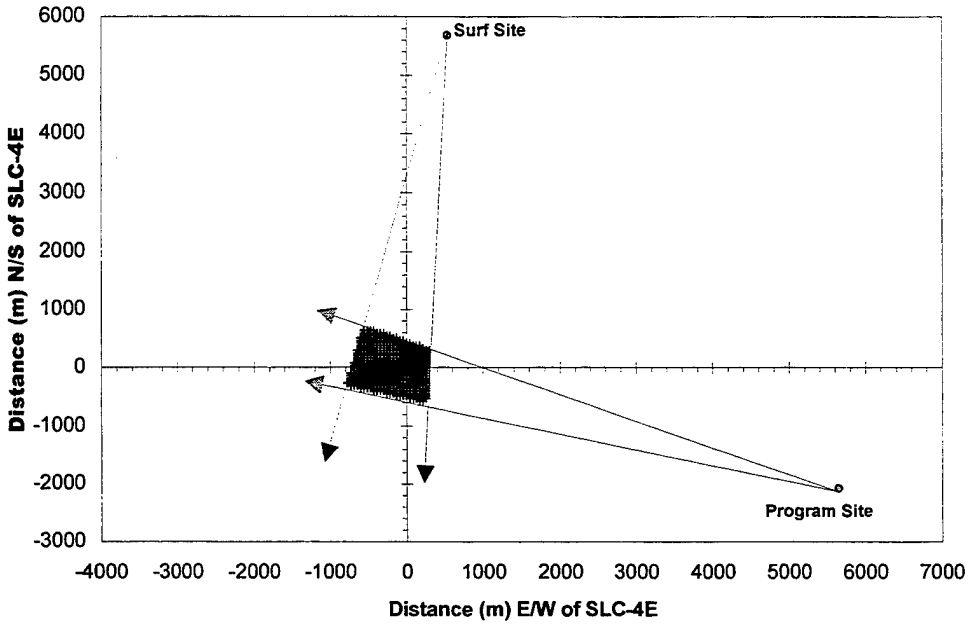


Figure 30. PLMVOL-derived Cartesian extent of abort cloud (T+78.378s).

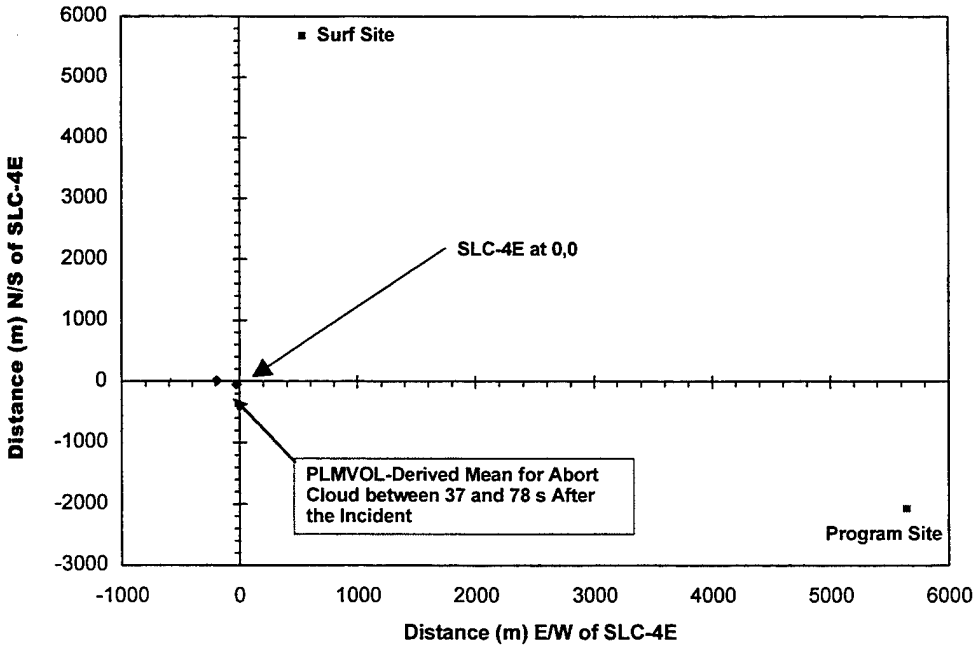


Figure 31. PLMVOL-derived abort cloud Cartesian coordinates (37 to 78s).

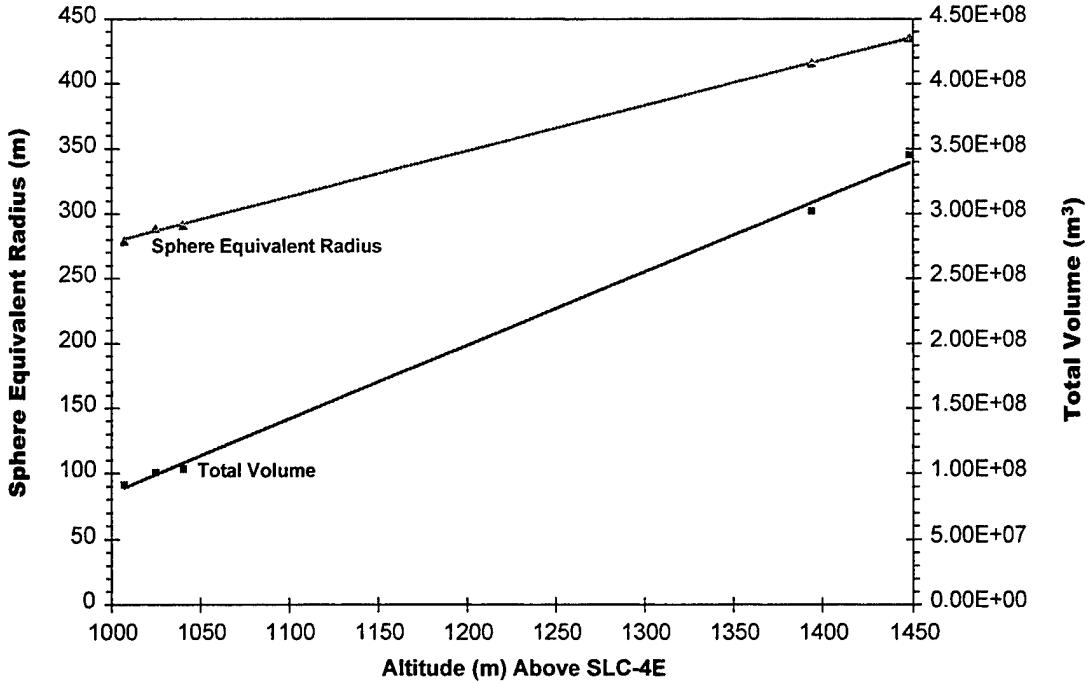


Figure 32. PLMVOL-derived sphere-equivalent radius and volume (37 to 78s).

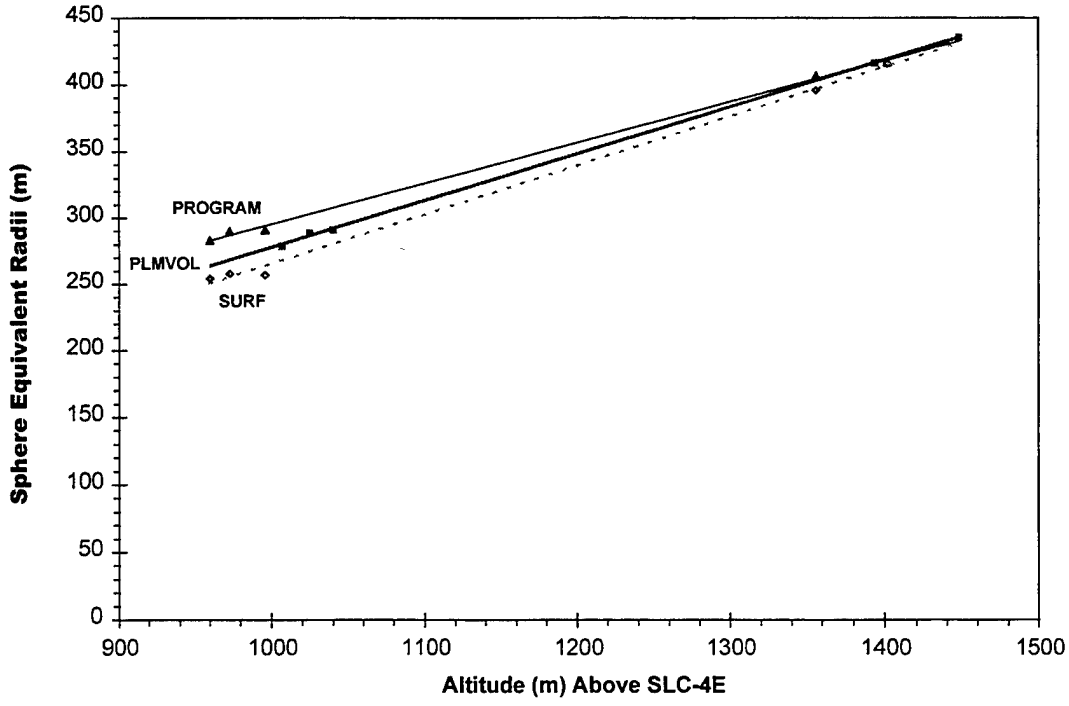


Figure 33. Sphere-equivalent radius: PLMVOL versus single site analyses (37 to 78s).

# 4. Conclusions

The quantitative analysis of the 34D-9 abort cloud imagery documented the abort cloud's growth, rise, and position for a couple of minutes after the first signs of SRM failure. Several analysis methods yielded similar results. When there was simultaneous imagery from multiple sites, PLMTRACK and PLMVOL image processing algorithms triangulated the cloud's extent and track. PLMVOL analysis also calculated the cloud's volume. These dual-site results validated the single-site analysis assumptions. The single-site analysis measured the cloud's rise, growth, and volume for more extensive periods of time than possible with the limited dual-site data. In addition to the imagery, the T-0.5 hour rawinsonde wind profiles provided information necessary for estimation of error bars for the single-site analysis assumption. The rawinsonde and imagery derived corrections for the abort cloud's distance from the Surf site enabled the best possible estimate for the air entrainment coefficient. The results of this analysis documented that the corrections were negligible and that even the simplest interpretation of the Surf site imagery provides a good estimate for the entrainment coefficient. The error analysis documented that the imagery-derived entrainment coefficient was 0.35 +/- 0.1 for the 34D-9 abort cloud. This value is similar to the imagery-derived entrainment coefficient measured for several normal Titan IV launches from CCAS. Therefore, the normal launch clouds and the single abort cloud are similar in regards to this important model parameter. However, the 34D-9 imagery-derived entrainment coefficient is 45% smaller than the default value (i.e., 0.64) used by REEDM version 7.08. The extrapolated "initial" abort cloud radius was 130m that was only 10% greater than REEDM version 7.08's value (i.e., 118m). This is good agreement for such an extrapolation.

The imagery-derived abort cloud characteristics documented in this report provide a useful test case for evaluating not only REEDM but also other dispersion models. Most dispersion models have multiple parameters that can be tuned within reasonable limits to "fit" observations. In addition to fitting the 34D-9 abort cloud behavior, the "tuned" model should also "fit" normal launch cloud observations.[1-10] Due to the complexities of terrain, meteorology, and physics, it is necessary to have an extensive set of test cases that encompass not only the terrain and physics but also the range of meteorological conditions that are considered viable for launches.

## References


1. R. N. Abernathy, R. A. Klingberg, and R. F. Heidner III, *Infrared and Visible Imagery of 19 January 1995 Peacekeeper Launch from Vandenberg Air Force Base,* Aerospace Report No.: TOR-95(5662)-2, The Aerospace Corporation, El Segundo, CA (01 May 1995).

2. Environmental Systems Directorate, *Ground Cloud Dispersion Measurements During the Titan IV #K23 (14 May 1995) at Cape Canaveral Air Station: Volume 1 – Test Overview and Data Summary,* Aerospace Report No. TR-96(1410)-1, SMC-TR-96-01, The Aerospace Corporation, El Segundo, CA (27 February 1996).

3. Environmental Systems Directorate, *Ground Cloud Dispersion Measurements During the Titan IV #K19 (10 July 1995) at Cape Canaveral Air Station,* Aerospace Report No. TR-96(1410)-3, SMC-TR-96-18, The Aerospace Corporation, El Segundo, CA (22 March 1996).

4. Environmental Systems Directorate, *Ground Cloud Dispersion Measurements During the Titan IV #K21 (6 November 1995) at Cape Canaveral Air Station,* Aerospace Report No. TR-96(1410)-4, SMC-TR-96-21, The Aerospace Corporation, El Segundo, CA (21 June 1996).

5. R. N. Abernathy, R. F. Heidner III, B. P. Kasper, and J. T. Knudtson, *Visible and Infrared Imagery of the Launch of Titan IV K-23 from Cape Canaveral Air Force Station on 14 May 1995,* Aerospace Report No. TOR-96(1410)-1, The Aerospace Corporation, El Segundo, CA (15 September 1996).

6. R. N. Abernathy, R. F. Heidner III, and K. L. Foster *Aircraft HCl Sampling of the Titan IV K-23 Launch Effluent Cloud,*" Aerospace Report No.TR-96(1410)-2, SMC-TR-96-22, The Aerospace Corporation, El Segundo, CA (15 September 1996).

7. Environmental Systems Directorate, *Ground Cloud Dispersion Measurements During The Titan IV Mission #K15 (5 December 1995) at Vandenberg Air Force Base, Volume 1 – Test Overview and Data Summary,* Aerospace Report No. TR-97(1410)-3, SMC-TR-97-05, The Aerospace Corporation, El Segundo, CA (10 February 1997).

8. Environmental Systems Directorate, *Ground Cloud Dispersion Measurements During the Titan IV #K16 (24 April 1996) at Cape Canaveral Air Station, Volume 1 – Test Overview and Data Summary,* Aerospace Report No. TR-97(1410)-4, SMC-TR-97-10, The Aerospace Corporation, El Segundo, CA (31 March 1997).

9. Environmental Systems Directorate, *Ground Cloud Dispersion Measurements During the Titan IV #K22 (12 May 1996) at Vandenberg Air Force Base, Volume 1 – Test Overview and Data Summary,* Aerospace Report No. TR-97(1410)-5, SMC-TR-97-18, The Aerospace Corporation, El Segundo, CA (30 June 1997).

10. Environmental Systems Directorate, *Ground Cloud Dispersion Measurements During the Titan IV Mission #K2 (3 July 1996) at Cape Canaveral Air Station, Volume 1 – Test Overview and Data Summary,* Aerospace Report No. TR-97(1410)-6, SMC-TR-97-19, The Aerospace Corporation, El Segundo, CA (15 July 1997).

## Appendix A — Acronyms and Abbreviations

| | |
|---|---|
| A-50 | Aerozine 50 |
| AGL | Above Ground Level (SLC-4E is ground level for the abort cloud) |
| Alt | Altitude in meters above specified reference (i.e., SLC-4E for 34D-9 cloud) |
| AZ | Azimuth clockwise from north |
| AZsurf | AZ in degrees clockwise from north as measured from Surf site |
| AZprog | AZ in degrees clockwise from north as measured from Program site |
| CCAS | Cape Canaveral Air Station |
| d | ellipsoid Diameter in specified Cartesian axis (E/W, N/S, or Vertical) |
| $d_{EW}$ | ellipsoid Diameter along East/West axis (determined by Surf (northern) perspective) |
| $d_{NS}$ | ellipsoid Diameter along North/South axis (determined by Program (eastern) perspective) |
| $d_V$ | ellipsoid Diameter along Vertical axis (determined by either Surf or Program perspectives) |
| dAZ | Difference in AZ between two objects in an image |
| dEL | Difference in EL between two objects in an image |
| dW | Difference in absolute Width (i.e., corrected for FOV) for an object observed in different images |
| dX | Difference in X pixel values between two pixels (i.e., objects in an image) |
| dY | Difference in Y pixel values between two pixels (i.e., objects in an image) |
| D | ground Distance between two objects |
| Dsurf | ground Distance between object and Surf site |
| Dprog | ground Distance between object and Program site |
| EL | Elevation of object relative to level |
| ELsurf | Elevation in degrees relative to level as measured from Surf site |
| ELprog | Elevation in degrees relative to level as measured from Program site |
| FOV | Field Of View of image in degrees horizontal or degrees vertical |
| GMT | Greenwich Mean Time |
| Ground Cloud | normal launch cloud that includes exhaust reflected from pad and launch column consumed by rising exhaust duct cloud |
| LBS | pounds |
| mean | weighted average of all values |
| middle | half way between the top and the bottom and half way between the left and the right |
| MSL | Mean Sea Level |
| MST | Mobile Service Tower at launch pad |
| MVP | Model Validation Program |

| | |
|---|---|
| N2O4 | dinitrogen tetroxide (i.e., hypergolic oxidizer) |
| PST | Pacific Standard Time |
| PSIA | Pounds per Square Inch Absolute |
| $r_{sphere}$ | Sphere-equivalent Radius |
| $r_{EW}$ | ellipsoid Radius along East/West axis as measured by Surf perspective |
| $r_{NS}$ | ellipsoid Radius along North/South axis as measured by Program perspective |
| $r_V$ | ellipsoid Radius along Vertical axis |
| REEDM | Rocket Exhaust Effluent Dispersion Model used at VAFB and CCAS |
| SLC | Space Launch Complex |
| SR | Slant Range between imagery site and observed feature |
| SRM | Solid Rocket Motor |
| TVC | Thrust Vector Control |
| UT | Umbilical Tower at launch pad |
| v(Surf) | wind Velocity component towards or away from Surf site |
| VAFB | Vandenberg Air Force Base |
| x | Cartesian coordinate in east/west direction relative to SLC-4E at x,y = 0,0 |
| X | "horizontal" pixel value (i.e., 0 at left of image and 640 at right of image) |
| y | Cartesian coordinate in north/south direction relative to SLC-4E at x,y = 0,0 |
| Y | "vertical" pixel value (i.e., 0 at bottom of image and 480 at top of image) |
| z | altitude relative to MSL (opposed to "Alt" which is relative to SLC-4E) |

## Appendix B — Angular to Absolute Dimensions

The diameter of the abort cloud is given by:

$$d = 2 \times D \times \tan(\frac{dAZ}{2}) = 2 \times SR \times \tan(\frac{dX \times hdpp}{2})$$

where "d" is the diameter of the abort cloud, "D" is the ground distance between the imagery site and the center of the abort cloud, and "dAZ" is the azumithal diameter (i.e., projected to the ground plane) of the cloud as observed from the imagery site. For the 34D-9 imagery from Surf site, "D" is approximately equal to the ground distance between SLC-4E and the imagery site. In the result's section, we used Program site imagery and rawinsonde data to estimate the errors associated with this approximation and showed that it was a good approximation. It is important to remember that "dAZ" is angular width measured in the ground plane and is only equal to the pixel width (dX) times the horizontal degrees per pixel (hdpp) when the object is in the ground plane. Therefore, one must use the slant range (SR) between the camera and the center of the cloud to calculate the cloud's diameter directly from the product of "dX" times "hdpp." Appendix C provides for trigonometric formulas for calculating "dAZ" for elevated objects.

The height of an abort cloud feature (i.e., top, bottom, left, right) above the ground plane of the imagery site is given by:

$H = D \times \tan(\mathrm{EL})$ where "H" is the height above the imagery site; "D" is the ground distance between the imagery site and the abort cloud feature; and "EL" is the elevation of the feature relative to level at the imagery site.

The altitude above ground level at SLC-4E is given by:

$\mathrm{Alt} = \mathrm{H} - d\mathrm{H}$ where "H" is the height above the imagery site and "dH" is the difference in height between SLC-4E ($H_{SLC4E}$) and the imagery site ($H_{SITE}$). Therefore, since SLC-4E is 91m higher than Surf site, an object has a lower "Alt" above SLC-4E than an "H" above Surf site.

$d\mathrm{H} = H_{SCL4E} - H_{SITE}$

The vertical diameter of the abort cloud is given by:

$d_V = Alt_{TOP} - Alt_{BOTTOM}$ where "$Alt_{TOP}$" is the altitude of the top and "$Alt_{BOTTOM}$" is the altitude of the bottom of the abort cloud.

## Appendix C — Trigonometric Interpretation of Imagery

Within a given row of pixels, the X pixels correspond to the Angle (A) of rotation within the plane that contains all pixels in that row. The plane has elevation $EL_p$ relative to level at the imagery site. The equations used in the trigonometric interpretation of the imagery are:

$X_c = 640/2$ where $X_c$ is the center horizontal pixel in the image

$Y_c = 480/2$ where $Y_c$ is the center vertical pixel in the image

$hdpp = FOV_h / 640$ where hdpp is the horizontal degrees per X pixel

$vdpp = FOV_v / 480$ where vdpp is the vertical degrees per Y pixel

$dA = (X_{ref} - X_c) \times hdpp$ where dA is the angular difference between the reference object and the center of the image within the same row of pixels (i.e., within a plane at ELp).

It can be shown that the elevation ($EL_p$) of the plane for the row of pixels that contains the reference object (i.e., at $EL_{ref}$) is given by:

$EL_p = \sin^{-1}(\sin(EL_{ref}) / \cos(dA))$ where $EL_p$ is the elevation for the row of pixels defined by $Y = Y_{ref}$. Therefore, ELp is equal to ELref when the reference object is along the center vertical line of the image. As the camera rotates away from the reference object, the elevation of the camera (i.e., ELp) must increase to keep the object within the same row of pixels. Therefore for ELref = 10 and dA = 10, ELp = 10.16. This is consistent with Figure 2 which illustrated that lines of constant elevation appear to curve upward towards the edges of the FOV.

For the center vertical line in the image, Y corresponds to elevation for any inclination of the camera. Therefore, one can calculate the elevation of the center pixel in the image using the following equation:

$$EL_c = EL_p + dY_{c-ref} \times vdpp = \sin^{-1}(\sin(EL_{ref}) / \cos(dA)) + (Y_c - Y_{ref}) \times vdpp)$$

It can also be shown that the difference in azimuth (i.e., angular difference in the ground plane) between the reference object and the center of the image within the same row of pixels is given by:

$$dAZ = AZ_{ref} - AZ_c = \tan^{-1}(\sin(dA) / (\cos(dA) \times \cos(EL_p))$$

when $EL_p$ = Zero $dAZ = dA$ (i.e., the linear treatment)

when $EL_p$ = 90 Degrees $dAZ \approx \infty$ (i.e., the trigonometric treatment fails)

It can also be shown that the azimuth to the center of the image is given by:

$$AZ_c = AZ_{ref} + dAZ = AZ_{ref} + \sin^{-1}(\sin(dA) / \cos(EL_{ref}))$$

For any pixel of interest (i.e., $X_i$,$Y_i$), one can calculate the $AZ_i$ and $EL_i$ using the following relationships:

$$AZ_i = AZ_c + dAZ_i = AZ_c + \tan^{-1}(\sin(dA_i) / (\cos(dA_i) \times \cos(EL_{pi}))$$

where dAi is the angular rotation from Xc to the selected Xi within the same row (i.e., Y=Yi):

$$dA_i = (X_i - X_c) \times hdpp$$

Therefore, as expected, the angle $dA_i$ increases to the right of the center and decreases to the left of the center. $EL_{pi}$ is the EL of the plane for the row of pixels that contains $Y_i$. Therefore:

$$EL_{pi} = EL_c + (Y_i - Y_c) \times vdpp$$

This linear interpretation of the Y pixels is valid for the center vertical line in the image and for pixels near the center of the image for low elevations. The elevation of a pixel Xi,Yi is given by:

$$EL_i = \sin^{-1}(\cos(dA_i) \times \sin(EL_{pi}))$$

As dAi approaches zero, $EL_i$ approaches $EL_{pi}$.

Using the above equations, it is possible to calculate the difference in AZ and EL between any two pixels in an image.

## Appendix D — Estimates for Restricted Perspectives

Figure 34 and Figure 35 illustrate the side perspective and the skyward perspective of an ellipsoid-shaped abort cloud from Surf site at T+129.883s (i.e., the last abort cloud image). In Figure 34, the ellipsoid has a 1.46 horizontal to vertical aspect ratio (as measured from Surf site) to illustrate possible restrictions in viewing the true vertical diameter from 5706m away and from a low elevation. In Figure 35, the cloud has equivalent north/south and east/west diameters consistent with earlier imagery from Program and Surf sites. The drawings are scaled to accurately reflect the angular extent of the cloud and, therefore, the magnitude of the errors for the last image (i.e., worst case).

Review of Figure 34 reveals a 6% overestimate for the vertical diameter (100% (918-870)/870) based upon the projected vertical diameter (918 m) and the actual vertical diameter (2 x 435m). Likewise, review of Figure 35 reveals a 3% overestimate of the horizontal diameter (100% (1318-1276)/1276) based upon the projected horizontal diameter (2 x 659m) and the actual horizontal diameter (2 x 638m). These values provide two estimates for the ellipsoid volume:

$$V' = \frac{4}{3} \times \pi \times (\frac{1318}{2})^2 \times \frac{918}{2} = 8.35E8$$

$$V = \frac{4}{3} \times \pi \times (\frac{1276}{2})^2 \times \frac{870}{2} = 7.42E8$$

This corresponds to a 13% overestimate in the cloud's volume. The sphere equivalent radius is:

$$r = \sqrt[3]{\frac{(V \times 3)}{4 \times \pi}}$$

Therefore, the two volumes correspond to radii ranging from 584m for V' to 562m for V. Thus the 13% overestimate in V corresponds to only a 4% overestimate in the sphere-equivalent radius. This is the worst case for Surf site since all earlier images are of smaller abort clouds at lower elevations.

Figure 36 reveals that the "middle" height (1909 m) above Surf site is also affected by perspective since there is more overshoot for the top than undershoot for the bottom of the cloud. This results in an apparent middle height of 1918 m ((1909+478)-(1909-440)). Subtracting 91 m from these heights converts them to altitudes above SLC-4E: 1818m and 1827, respectively. This is only a 0.5% overshoot (100% (1827-1818)/1818) in altitude.

There should be a slight overestimate of the entrainment coefficient since the overestimation of the sphere-equivalent radius is greater for higher altitudes than for lower altitudes. In contrast, there is a smaller overshoot for the altitude of the cloud. Thus, the slope of sphere-equivalent radius versus altitude would be too steep (i.e., overestimation of entrainment coefficient). If this were a substantial error, there would be upward curvature for the radius versus altitude plot at higher altitudes. This does not appear to be the case for the 34D-9 imagery as revealed by Figure 19.

One can estimate the effect of these errors on the calculated entrainment coefficient by using a radius of 210m for the cloud at 800m altitude and calculating the slope for a plot of radius versus altitude by using the range of radii and altitudes for the highest altitude. This yields a ratio (i.e., slope) of 0.346 [i.e., (562-210)/(1818-800)] for the smallest values and only 0.364 [i.e., (584-210)/(1827-800)] for the largest values. Therefore, the entrainment coefficient is 0.35 +/- 0.01.

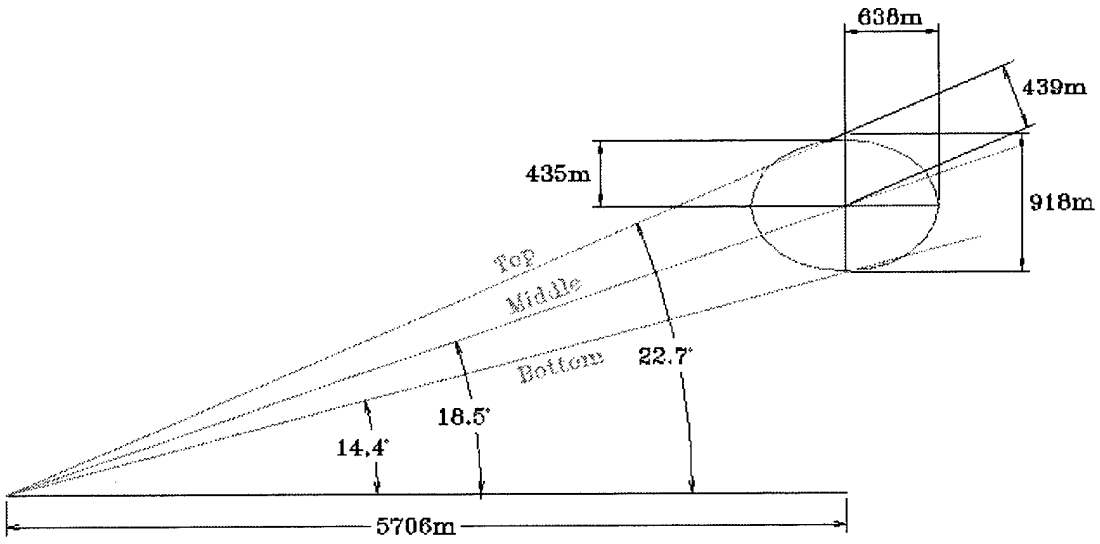


Figure 34. Elevation angles and side perspective for surf site (T+129.830s).

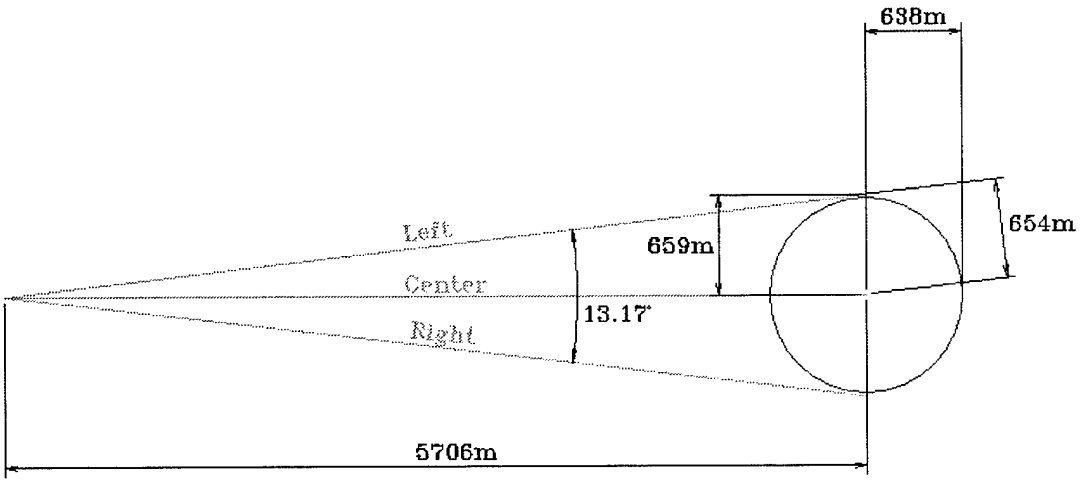


Figure 35. Azimuthal angle and skyward perspective for surf site (T+129.830s).

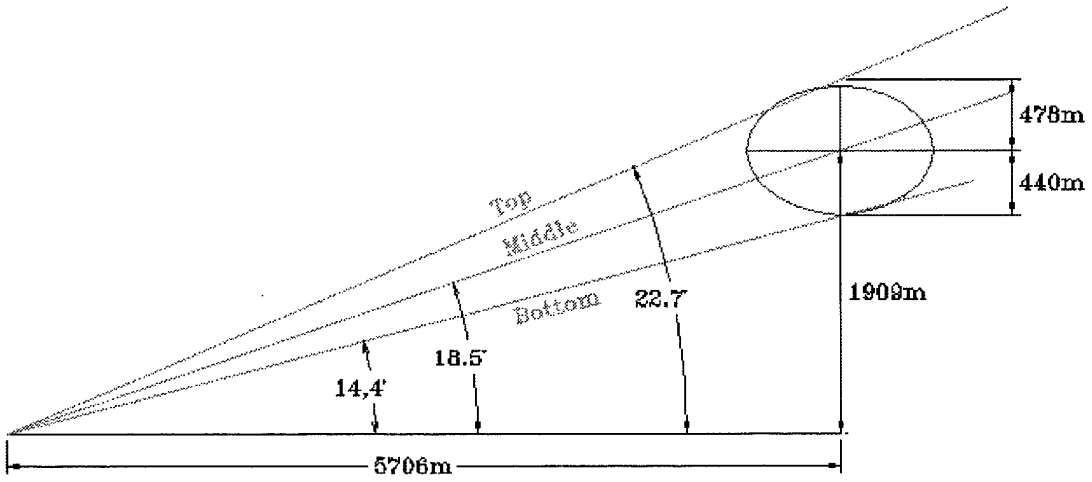


Figure 36. Altitude errors from side perspective for surf site (T+129.830s).

# Appendix E — T-0.5 Hour Rawinsonde Input for REEDM

```
$ 04/18/86
NEW TITAN RAWINSONDE FROM FILE ar1815   WRITTEN TO FILE NAMED raw1815.new
TEST NBR: T-0.5H
BLDG     , VANDENBERG AFB, CALIF.
RAWINSONDE RUN RECOSTRUCTED BY GEODYNAMICS
tZULU  DD MON YYYY   P          CC         CH
1815Z  18 APR 1986   *          0.0        9999.0
ASCENT NBR 1815
   ALT   DIR  SPD   TEMP     DPT    PRESS  RH ABHUM  DENSITY
GEOMFT   DEG  KTS  DEG C  DEG C     MBS PCT  G/M3   G/M3

   367. 330.   8.   16.5    7.7 1007.50  56. 99.0  1206.98
   473. 339.  13.   12.2    3.9 1004.00  57. 99.0  1222.02
   574. 341.  12.   12.6    4.3 1000.00  57. 99.0  1215.33
  1119. 354.   6.   14.9    6.1  980.44  56. 99.0  1181.35
  1292.   6.   6.   15.7    6.7  974.00  55. 99.0  1170.23
  1940.  31.   4.   13.1    3.6  949.81  53. 99.0  1152.50
  2439.  54.   6.   11.4    1.6  935.00  51. 99.0  1141.55
  2874.  68.   4.   13.0     .3  920.00  42. 99.0  1117.19
  3733. 107.   6.    9.8   -2.7  891.33  41. 99.0  1094.95
  4604. 119.  11.    6.7   -5.7  863.56  41. 99.0  1073.22
  5029. 122.  13.    5.1   -7.2  850.00  41. 99.0  1062.54
  5491. 125.  14.    3.6   -8.5  835.00  41. 99.0  1049.58
  6384. 132.  10.    2.7  -10.2  808.15  38. 99.0  1019.40
  7232. 141.   3.    1.7  -11.8  782.15  36. 99.0   990.10
  8089.  20.   6.     .8  -13.5  757.00  33. 99.0   961.63
  8988.  13.  16.    2.3  -27.7  732.00   9. 99.0   925.51
  9903.  16.  20.    1.8  -19.2  707.26  19. 99.0   895.62
 10170.  17.  21.    1.6  -16.6  700.00  24. 99.0   886.79
 10866.  19.  23.     .7  -17.3  682.00  24. 99.0   866.85
 11864.  14.  25.    -.8  -18.1  657.16  25. 99.0   839.99
 12836.   9.  22.   -2.4  -19.0  633.22  26. 99.0   813.99
 13802.  11.  19.   -3.9  -19.8  610.16  28. 99.0   788.81
 14817.   9.  22.   -5.4  -20.7  587.93  29. 99.0   764.44
 15780.   4.  26.   -6.9  -21.5  566.52  30. 99.0   740.85
 16708.   3.  28.   -8.5  -22.4  545.88  31. 99.0   718.01
 17563. 359.  27.  -10.0  -23.2  526.00  33. 99.0   695.89
 18478. 349.  27.  -11.9  -25.1  507.29  32. 99.0   676.16
 18842. 347.  28.  -12.7  -25.8  500.00  32. 99.0   668.43
 19358. 344.  29.  -13.8  -26.7  489.73  32. 99.0   657.52
 20191. 343.  30.  -15.7  -28.3  473.08  33. 99.0   639.76
 21070. 345.  26.  -17.5  -29.8  457.00  33. 99.0   622.50
 21990. 359.  24.  -20.0  -32.3  438.92  32. 99.0   603.93
 22899.  11.  27.  -22.6  -34.8  421.55  31. 99.0   585.97
 23938.  11.  29.  -25.1  -37.3  404.87  31. 99.0   568.59
 24291.  10.  30.  -25.9  -38.1  400.00  30. 99.0   563.49
 24993.   8.  31.  -27.7  -39.4  388.32  31. 99.0   550.97
 26058.   4.  32.  -30.2  -41.4  372.22  32. 99.0   533.60
 27095.   6.  31.  -32.7  -43.3  356.79  33. 99.0   516.84
EOF
EOT
```

## TECHNOLOGY OPERATIONS

The Aerospace Corporation functions as an "architect-engineer" for national security programs, specializing in advanced military space systems. The Corporation's Technology Operations supports the effective and timely development and operation of national security systems through scientific research and the application of advanced technology. Vital to the success of the Corporation is the technical staff's wide-ranging expertise and its ability to stay abreast of new technological developments and program support issues associated with rapidly evolving space systems. Contributing capabilities are provided by these individual Technology Centers:

**Electronics Technology Center:** Microelectronics, VLSI reliability, failure analysis, solid-state device physics, compound semiconductors, radiation effects, infrared and CCD detector devices, Micro-Electro-Mechanical Systems (MEMS), and data storage and display technologies; lasers and electro-optics, solid state laser design, micro-optics, optical communications, and fiber optic sensors; atomic frequency standards, applied laser spectroscopy, laser chemistry, atmospheric propagation and beam control, LIDAR/LADAR remote sensing; solar cell and array testing and evaluation, battery electrochemistry, battery testing and evaluation.

**Mechanics and Materials Technology Center:** Evaluation and characterization of new materials: metals, alloys, ceramics, polymers and composites; development and analysis of advanced materials processing and deposition techniques; nondestructive evaluation, component failure analysis and reliability; fracture mechanics and stress corrosion; analysis and evaluation of materials at cryogenic and elevated temperatures; launch vehicle fluid mechanics, heat transfer and flight dynamics; aerothermodynamics; chemical and electric propulsion; environmental chemistry; combustion processes; spacecraft structural mechanics, space environment effects on materials, hardening and vulnerability assessment; contamination, thermal and structural control; lubrication and surface phenomena; microengineering technology and microinstrument development.

**Space and Environment Technology Center:** Magnetospheric, auroral and cosmic ray physics, wave-particle interactions, magnetospheric plasma waves; atmospheric and ionospheric physics, density and composition of the upper atmosphere, remote sensing, hyperspectral imagery; solar physics, infrared astronomy, infrared signature analysis; effects of solar activity, magnetic storms and nuclear explosions on the earth's atmosphere, ionosphere and magnetosphere; effects of electromagnetic and particulate radiations on space systems; component testing, space instrumentation; environmental monitoring, trace detection; atmospheric chemical reactions, atmospheric optics, light scattering, state-specific chemical reactions and radiative signatures of missile plumes, and sensor out-of-field-of-view rejection.